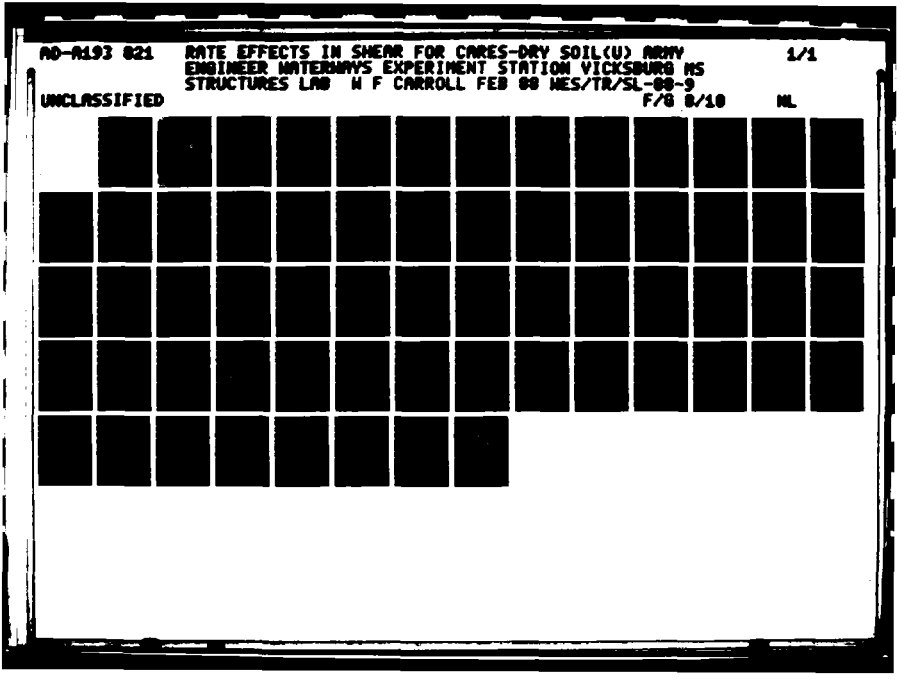
AD-A193 021
RATE EFFECTS IN SHEAR FOR CARES-DRY SOIL(U) ARMY ENGINEER WATERWAYS EXPERIMENT STATION VICKSBURG MS STRUCTURES LAB W F CARROLL FEB 88 WES/TR/SL-88-9
1/1
UNCLASSIFIED
F/G 8/10
NL

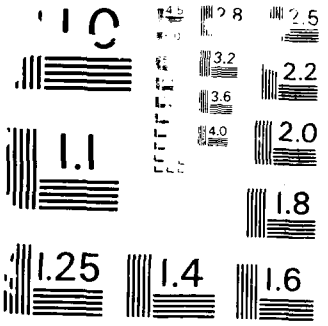

COPY RESOLUTION TEST CHART
NATIONAL BUREAU OF STANDARDS - 1961

DTIC FILE COPY

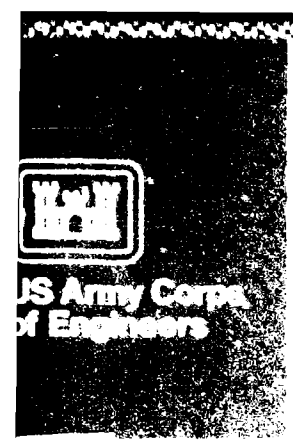

AD-A193 021

[illegible]

[illegible]

DTIC
ELECTE
MAR 2 4 1988
S D
D

February 1988

Final Report

[illegible]

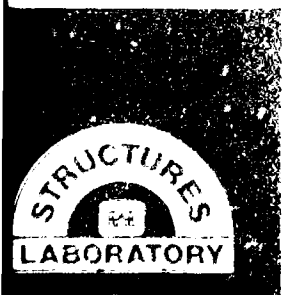

88 3 23 030

Unclassified

SECURITY CLASSIFICATION OF THIS PAGE

REPORT DOCUMENTATION PAGE

Form Approved
OMB No 0704-0188
Exp Date Jun 30 1986

1a REPORT SECURITY CLASSIFICATION Unclassified	1b RESTRICTIVE MARKINGS
2a SECURITY CLASSIFICATION AUTHORITY	3 DISTRIBUTION/AVAILABILITY OF REPORT Approved for public release; distribution unlimited.
2b DECLASSIFICATION/DOWNGRADING SCHEDULE	
4 PERFORMING ORGANIZATION REPORT NUMBER(S)	5 MONITORING ORGANIZATION REPORT NUMBER(S) Technical Report SL-88-9
6a NAME OF PERFORMING ORGANIZATION University of Central Florida 6b OFFICE SYMBOL (If applicable)	7a NAME OF MONITORING ORGANIZATION USAEWES Structures Laboratory
6c ADDRESS (City, State, and ZIP Code) Orlando, FL 32816	7b ADDRESS (City, State, and ZIP Code) PO Box 631 Vicksburg, MS 39180-0631
8a NAME OF FUNDING/SPONSORING ORGANIZATION US Army Corps of Engineers 8b OFFICE SYMBOL (If applicable)	9 PROCUREMENT INSTRUMENT IDENTIFICATION NUMBER
8c ADDRESS (City, State, and ZIP Code) 20 Massachusetts Ave., NW Washington, DC 20314-1000	10 SOURCE OF FUNDING NUMBERS PROGRAM ELEMENT NO: PROJECT NO: 4A161102AT22; TASK NO: BO; WORK UNIT ACCESSION NO: 005

11 TITLE (Include Security Classification)
Rate Effects in Shear for CARES-Dry Soil

12 PERSONAL AUTHOR(S)
Carroll, William F.

13a TYPE OF REPORT	13b TIME COVERED	14 DATE OF REPORT (Year, Month, Day)	15 PAGE COUNT
Final report	FROM _____ TO _____	February 1988	62

16 SUPPLEMENTARY NOTATION
Available from National Technical Information Service, 5285 Port Royal Road, Springfield, VA 22161.

17 COSATI CODES			18 SUBJECT TERMS (Continue on reverse if necessary and identify by block number)	
FIELD	GROUP	SUB-GROUP	CARES-Dry clayey sand	Shear strength
			Dynamic soil properties	Stress-strain
			Loading rate effects	Triaxial shear tests

19 ABSTRACT (Continue on reverse if necessary and identify by block number)

Thirty-six individual specimens of CARES-Dry soil were tested in the fast triaxial shear device (FTRXD) at three confining pressures and at six test velocities. The slowest were static, unconsolidated, undrained triaxial tests. The fastest (9.0 ips) were the fastest that could be obtained while maintaining constant deformation velocity.

The FTRXD performed well. Load and displacement as a function of time were measured accurately. Constant velocities were achieved. Procedures developed to prepare specimens, mount them in the FTRXD, and assemble and operate the FTRXD were reasonably efficient.

The new upper load cell was accurate, durable, and easy to use. During this test series, discrepancies between the upper and lower load cells were essentially eliminated, due in part to the new upper load cell.

Neither the dynamics of the FTRXD nor specimen inertia influenced the test (Continued)

20 DISTRIBUTION/AVAILABILITY OF ABSTRACT	21 ABSTRACT SECURITY CLASSIFICATION
☒ UNCLASSIFIED/UNLIMITED ☒ SAME AS RPT ☐ DTIC USERS	Unclassified
22a NAME OF RESPONSIBLE INDIVIDUAL	22b TELEPHONE (Include Area Code) / 22c OFFICE SYMBOL

DD FORM 1473, 84 MAR — 83 APR edition may be used until exhausted. All other editions are obsolete.

SECURITY CLASSIFICATION OF THIS PAGE
Unclassified

19. ABSTRACT (Continued).

results noticeably, despite the fact that some specimens were brought to failure in 2 to 3 msec. In the fastest tests, a small lag in the response of the lower load cell occurred, the time it took for a disturbance at the top of the specimen to propagate to the bottom. Thus using faster test velocities or longer test specimens will require that specimen inertia be taken into account.

The FTRXD does permit assessing rate effects of soils subjected to triaxial shear throughout meaningful ranges of principal stress difference and nominal axial strain. During deformation, the CARES-Dry soil appeared to pass through three behavior modes: initial grain structure response, grain structure collapse, and plastic shear failure.

During the first mode, the grain structure of the specimen is intact and the relationship between principal stress difference and nominal axial strain is essentially linear, increases predictably with increasing confining pressure, and is unaffected by deformation velocity at high confining pressure. At low confining pressure when deformation velocity is high, specimen behavior was variel and inconclusive.

The second and third modes show the same effects from deformation velocity. The relationship between principal stress difference and nominal axial strain is highly nonlinear during the second mode but approaches linearity during the third. In both modes increasing confining pressure increases the magnitudes of principal stress difference in a predictable manner, and there is a modest increase in the magnitude of principal stress difference at high confining pressure due to deformation velocity. No rate effects were observed in these modes at lower confining pressures.

The CARES-Dry soil at the moisture content and dry density tested has linear Coulomb failure envelopes. The envelopes were different for different nominal axial strains but were unaffected by deformation velocity within the range of the test series parameters.

PREFACE

The Geomechanics Division of the Structures Laboratory (SL) at the US Army Engineer Waterways Experiment Station (WES) designed and constructed a fast triaxial shear device (FTRXD) and is currently evaluating it under the sponsorship of the Office, Chief of Engineers, US Army, as a part of Project 4A161102AT22, Task BO, Work Unit 005, "Constitutive Properties for Natural Earth and Manmade Materials." The current evaluation focusses on the conduct of rapid tests on soil specimens with the device to ascertain possible rate effects in the soil, continuing analysis of the dynamics of the FTRXD itself, and modifying the FTRXD as appropriate to improve its capability to measure the engineering properties of geotechnic materials subjected to loads which cause failure in less than 1 millisecond.

Responsibility for the evaluation was assigned to Mr. John Ehrgott, Geomechanics Division (GD), SL, under the general direction of Dr. J.G. Jackson, Jr., Chief, GD, SL. The conduct of the testing and the evaluation of the results were undertaken by Dr. William F. Carroll, Professor of Engineering at the University of Central Florida (UCF) in Orlando, FL, under an Intergovernmental Personnel Act (IPA) agreement with WES. This report was prepared by Dr. Carroll.

Dr. David R. Jenkins is Chair, Department of Civil Engineering and Environmental Sciences at UCF. Dr. Robert D. Kersten was Dean of the College of Engineering when the testing was performed.

The Commander and Director of WES is COL Dwayne G. Lee, CE. The Technical Director is Dr. Robert W. Whalin. Mr. Bryant Maher is Chief, SL.

DTIC
COPY
INSPECTED
1

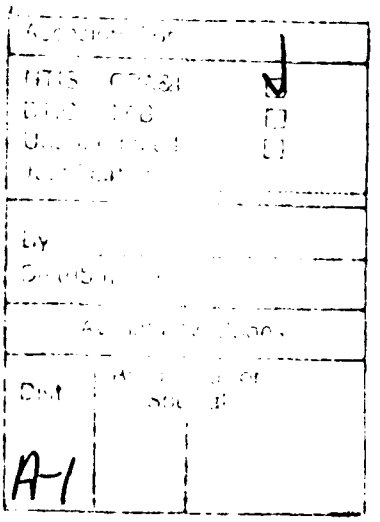

CONTENTS

CONVERSION FACTORS, NON-SI TO SI (METRIC)
UNITS OF MEASUREMENT

Non-SI units of measurement used in this report can be converted to SI (metric) units as follows:

Multiply	By	To Obtain
feet	0.3048	metres
inches	25.4	millimetres
inches per second	0.0254	metres per second
mils	0.0254	millimetres
pounds (force)	4.448222	newtons
pounds (force) per square inch	0.006894757	megapascals
pounds (mass)	0.4535924	kilograms
pounds (mass) per cubic inch	16.01846	kilograms per cubic metre

RATE EFFECTS IN SHEAR FOR CARES-DRY SOIL

CHAPTER 1

INTRODUCTION

1.1 BACKGROUND

The evaluation and development of the U.S. Army Engineer Waterways Experiment Station (WES) Fast Triaxial Shear Device (FTRXD) is ongoing. This effort progressed sufficiently by early 1987 to permit the conduct of a test program with the FTRXD which could determine rate effects in shear in a soil and demonstrate further the ability of the device to address the constitutive behavior of soils at stress levels near failure. The device itself is described in detail and its evaluation to this point presented in Reference 1.

1.2 PURPOSE AND SCOPE

The purpose of this report is to describe the test program run on CARES-Dry soil with the FTRXD, to present the quantitative results of the testing, to analyze these results, and to assess the performance of the FTRXD. In Chapter 2, the test plan and specimen preparation are described. The results of the testing are presented and analyzed in Chapter 3, and some conclusions are drawn and recommendations made in Chapter 4.

CHAPTER 2

TEST PLANNING AND PREPARATION

2.1 THE CARES-DRY SOIL

All of the evaluation testing with the FTRXD to date has been done on CARES-Dry soil, a clayey sand which classifies as SC in the Unified Soil Classification System. Some of this testing is described in Reference 1. Definitive testing of the CARES-Dry soil has been accomplished at WES to determine its index and standard engineering properties. These results are presented in Reference 2. Moreover, testing for rate effects in the CARES-Dry soil has been performed in one-dimensional compression using the WES 0.1-msec uniaxial strain compression testing device and is presented in Reference 3. As a consequence, CARES-Dry soil was chosen for the first test series with the FTRXD to determine, if possible, rate effects in shear for the CARES-Dry soil.

To permit the possibility for comparisons of rate effects in shear of the CARES-Dry soil with those exhibited by it during the earlier one-dimensional compression rate testing, an effort was made to achieve moisture contents and dry densities during the FTRXD testing which were comparable to those achieved during the one-dimensional testing. These moisture contents of about 3.5% and dry densities of about 115 pcf* were the target values adopted for the FTRXD test series.

2.2 THE TEST PLAN

Earlier evaluation of the FTRXD showed that to achieve a constant velocity during the deformation and loading of the FTRXD specimen, the FTRXD should be operated with oil in the lower chamber of the loading assembly, and the oil's rate of flow from this chamber during the testing should be controlled. When operated without this oil to achieve the very fast rates, specimen deformation occurred at a variable velocity and there were circumstances when the results were not fully understood. Consequently, the FTRXD device was operated during this test series with oil in the lower chamber of the loading assembly. The fastest velocities attained were about 9.0 inches per second (ips); the slowest were about 0.003 ips. Four additional intermediate velocities were also used to define specimen properties over the range of possible velocities which can be obtained when operating the FTRXD as described. These were nominally 0.15 ips, 0.3 ips, 1.0 ips, and 2.5 ips.

The CARES-Dry soil showed marked effects from confining pressure in earlier testing using confining pressures of

---

* A table of factors for converting non-SI units of measurement to SI (metric) units is presented on page iii.

50, 100, and 200 psi. The effects of confining pressure on specimen stiffness and strength were also noted in the earlier evaluation of the FTRXD to influence the dynamic response of the FTRXD. Moreover, whether or not confining pressure influences the rate effects was open to question. Thus some variation of confining pressure during the test series was considered important. The confining pressures adopted were 50, 100, and 200 psi.

In summary, the plan was to test identical specimens of the CARES-Dry soil prepared with a moisture content of 3.5% and dry density of 115 pcf. Tests were run at confining pressures of 50, 100, and 200 psi, and at test velocities of 0.003, 0.15, 0.3, 1.0, 2.5, and 9.0 ips. The six velocities chosen corresponded to nominal times to 15% nominal axial strain of 80 sec, 2 sec, 900 msec, 250 msec, 100 msec, and 25 msec.

To improve the reliability of the data and assess the repeatability of test results, each test was duplicated. The result was that 36 tests were conducted as 18 pairs of tests in which the pairs were intended to be identical. What was actually achieved is summarized in columns 4 through 8 of Table 2.1.

2.3 SPECIMEN PREPARATION

About 30 pounds of CARES-Dry soil, which passes the number 8 sieve, was premixed in mid-May to achieve a moisture content of about 3.5%. The mix was stored in a plastic bag which in turn was stored in a second plastic bag; these were stored in a metal container. Both bags and the container were each sealed separately. Sampling a few days after mixing revealed that the moisture content was 3.4%. Moisture content sampling during the test period in June and the moisture contents determined from FTRXD test specimens in June indicated that the moisture content for the test series was 3.2%. These latter 36 moisture contents are listed in column 4 of Table 2.1.

The soil was compacted in a special mold in three lifts to achieve the target dry density in a specimen 0.75 inches in diameter and 1.5-inches high. To this end, three equal amounts of the mix (7.25 gm) were precisely weighed. The first amount of soil was then poured into the mold and compressed with a 0.75-inch-diameter ram and the Universal Testing Machine until the soil in the mold was 0.50-inches high. The amount of compression was controlled by stopping the ram at a predetermined mark which indicated it had moved to the desired distance above the bottom of the mold. The top of this lift was scarified and the second amount of soil was poured into the mold and compressed until the soil in the mold was 1.00-inches high. The top of this second lift

was scarified, and the remaining amount of soil was poured into the mold and compressed until the soil in the mold was 1.50-inches high. The mold guides were then removed, and the specimen pushed on through the mold by the ram. Approximately 1200 pounds of force was required to compress each lift, and about 800 pounds was needed to push the specimen from the mold.

The specimen was then weighed and its diameter and height measured. Once its moisture content was determined after testing, its dry density was computed. Height, diameter, and dry density data for each specimen are shown on Table 2.1.

The dry densities achieved were about 118.5 pcf, 3.5 pcf higher than the target dry density. Early in the test period when sample preparation and testing procedures were being developed, it became apparent that the CARES-Dry soil prepared as a 0.75-inch-diameter by 1.5-inch-high specimen at a moisture content of 3.1-3.4% and a dry density of 115 pcf was too fragile to obtain consistent FTRXD test results without extraordinarily careful handling and specialized equipment. By increasing the dry density to 118-119 pcf, the soil as mixed, the equipment available, and reasonably simple handling procedures could be used. In the course of preparing about 50 specimens for the test series, equipment and procedures were refined and experience gained which might now permit more effective handling of specimens at moisture contents of 3.5% and dry densities of 115 pcf.

Immediately after the specimen was weighed and measured, it was mounted between the detachable upper and lower caps of the FTRXD upper and lower load cells. Two rubber membranes were carefully placed over the specimen and sealed to the caps with rubber bands. Finally a thin layer of gage coat was painted all over the membranes to protect them from the oil used in the FTRXD confining chamber and to aid in sealing the specimen from the confining pressure used during the test. The double membranes and the gage coat were necessary to prevent leakage from occurring while the specimen was immersed in the chamber oil under the confining pressure and before it was loaded, a period of time usually less than 5 minutes and always less than 10 minutes.

The entire specimen preparation procedure from opening the metal container with soil mix to installing the rubber membranes was done as quickly as possible and with the soil as covered as possible to minimize the loss of moisture from the specimen by evaporation. Because the specimens were small and contained only a very small amount of moisture (about 4 gm), even a small evaporation loss could be significant.

2.4 THE FTRXD

The FTRXD and the way it operates, and the instrumentation it uses have been described in detail in Reference 1. However, two small but important improvements were made to it for the test series reported here, in response to the recommendations made in Reference 1.

The cantilever target for the Kaman displacement gage was redesigned. It was reshaped from flat aluminum plate 1.00-inches wide by 0.385-inches thick and 1.625-inches long to a tapered aluminum target. The taper was in plan from 1.00 inches near the ram to 0.50 inches at the outer end, and in thickness from 1.18 inches at the ram to 0.72 inches at the outer end while keeping the top surface horizontal. The length was increased to 1.92 inches. The new cantilever target has a calculated period of 0.05 msec; the old one had a calculated period of about 0.20 msec and a period deduced from the evaluation testing of 0.25 msec. The thicker new target achieves greater fixity at the ram than the old one did.

The upper load cell was redesigned also. The new load cell uses a force washer instead of a hollow steel cylinder. The result is a greatly reduced natural period from the 0.11 msec period of the old upper load cell. It also eliminated the consistent, rate-dependent discrepancy in the readings of the upper and lower load cells.

TABLE 2.1

SUMMARY of SPECIMEN DATA and TEST PARAMETERS

Test	Height (in)	Diameter (in)	Moisture Content (%)	Dry Density (pcf)	Confining Pressure (psi)	Nominal Duration (msec)	Piston Velocity (ips)
X31	1.496	0.756	3.2	119	50	80000	0.0049
X34	1.488	0.755	3.1	119	50	80000	0.0044
X32	1.508	0.754	3.4	118	100	80000	0.0045
X35	1.500	0.755	3.1	119	100	80000	0.0035
X33	1.498	0.755	3.1	118	200	80000	0.0034
X36	1.503	0.755	3.3	118	200	80000	0.0033
X39	1.507	0.756	3.1	118	50	2000	0.16
X41	1.507	0.755	3.1	118	50	2000	0.16
X10	1.492	0.754	3.2	120	100	2000	0.12
X12	1.495	0.754	3.4	120	100	2000	0.14
X38	1.504	0.755	3.1	118	200	2000	0.16
X42	1.496	0.755	3.2	119	200	2000	0.15
X18	1.503	0.756	3.1	118	50	900	0.31
X37	1.502	0.755	3.1	119	50	900	0.37
X11	1.497	0.751	3.3	120	100	900	0.33
X15	1.496	0.757	3.5	118	100	900	0.31
X16	1.492	0.756	3.5	119	200	900	0.24
X17	1.508	0.754	3.1	118	200	900	0.28
X29	1.500	0.756	3.2	119	50	250	1.07
X30	1.503	0.753	3.2	118	50	250	1.09
X19	1.514	0.755	3.0	117	100	250	1.07
X27	1.500	0.755	3.1	118	100	250	1.04
X20	1.503	0.755	3.3	118	200	250	0.84
X28	1.490	0.756	3.1	119	200	250	0.85
X21	1.495	0.755	3.1	119	50	100	2.3
X24	1.496	0.756	3.1	119	50	150	1.5
X22	1.497	0.757	3.2	118	100	100	2.3
X25	1.509	0.755	3.1	118	100	100	2.5
X23	1.510	0.756	3.0	117	200	100	2.6
X26	1.495	0.754	3.3	119	200	100	2.4
X48	1.499	0.756	3.1	118	50	25	9.3
X49	1.515	0.756	3.1	118	50	25	8.6
X43	1.504	0.754	3.3	119	100	25	9.2
X46	1.505	0.756	3.1	118	100	25	9.5
X44	1.503	0.755	3.2	119	200	25	9.2
X47	1.501	0.756	3.1	118	200	25	8.9
Avg	1.501	0.755	3.18	118.5			
Std Dev	0.006	0.001	0.12	0.7			

CHAPTER 3

TEST RESULTS

3.1 GENERAL

The basic data which the FTRXD provides is load measured at the top of the specimen as a function of time by the upper load cell, load measured at the base of the specimen as a function of time by the lower load cell, and the downward displacement of the top of the specimen measured as a function of time by the Kaman displacement gage. The constant confining pressure imposed on the specimen during the test is monitored by a pressure gage.

The FTRXD was operated with oil in the lower chamber of the load cylinder in order to achieve constant velocity of the top of the specimen during the test. The flow of oil from this chamber was initiated with the rapid opening of a solenoid valve and regulated by a ball valve. Both upper and lower limits were imposed on the test velocities by the equipment and this manner of using it. The upper limit occurred because the pressure in the upper chamber of the load cylinder was limited to 1000 psi. Moreover, the size of the tubing leading from the lower chamber of the load cylinder, its constrictions, and the size of the openings in the solenoid and ball valves when wide open all imposed limits on the rate at which the oil could exit from the lower chamber of the load cylinder. The fastest velocities obtained (9.0 ips) occurred when most of the tubing and the ball valve were removed, and the pressure in the upper chamber was 1000 psi. The lower limit occurred when the opening in the ball valve was small enough to restrict the rate of oil flow so that its pressure in the lower chamber was not different enough from the pressure in the upper chamber to smoothly overcome the friction in the load assembly and the resistance which the specimen could offer to deformation.

Because the amount of specimen deformation to failure was small, usually less than 0.060 inches (60 mils), and a corresponding finite amount of time was required to get the FTRXD piston-ram up to speed after opening the solenoid valve, each test was initiated with the piston-ram backed away 0.10 inches (100 mils) from the specimen and upper load cell. This procedure ensured that constant velocities occurred during testing. However, it also required that considerable care be taken in mounting the specimen in the FTRXD and in assembling the device so that the specimen was aligned with the piston-ram. Some amount of "impact" necessarily occurred when the piston-ram first contacted the upper load cell and specimen; however, for the rates at which these tests were run, its effects were not noticeable.

The good alignment of specimens with the piston-ram was verified visually before each test and by examining the deformed specimens after testing. All specimens deformed symmetrically, most by bulging in the central one-third to one-half of the specimen height. Five of the 36 specimens exhibited clearly defined shear planes and these occurred when test velocities were slow -- nominally 0.003, 0.15, and 0.3 ips. The testing imposed a final deformation on each specimen of slightly more than 20% nominal axial strain (0.3 inches).

3.2 LOAD-TIME-DISPLACEMENT

The measured load at the top and base of the specimen and the measured displacement of the top of the specimen for each test are plotted against time on Figures 3.1 to 3.18. Each figure contains two graphs, one for each of the intended identical test pairs. The load scale in each case is the same to facilitate comparisons. The time scales are the same for each nominal velocity, also to facilitate comparison. Each graph indicates the important test parameters such as confining pressure, velocity to failure, moisture content, and dry density. Although it was only possible to achieve approximately a specific value of test velocity, it is clear from a visual examination of the linearity of the displacement-time plots of all tests that a constant velocity was accurately achieved for each test, and especially from the onset of specimen deformation until its peak load occurred.

Figures 3.1 to 3.6 show the load-displacement-time data for the tests run at a confining pressure of 50 psi. At all velocities the load-time plots exhibited the same shape. Given the linearity of the displacement-time plots, the shape of the load-time, load-displacement, or principal stress difference (PSD) - nominal axial strain (NAS) curves will all be the same for a particular test. The load curves are very linear up to 80-90% of the peak load. The peak load is well-defined at 140-150 lbs, and load after the peak falls off gradually.

The readings from the upper and lower load cells were nearly identical in most of the tests. In some instances the upper load cell read higher, and in some it was the lower load cell that read higher. In either case, the discrepancy between upper and lower load cells was small, especially prior to the occurrence of the peak load. The most important factor affecting the discrepancy of the load cell readings was the determination of where and when the readings started. In each test this was done very carefully. Usually the sharpest indication that the specimen was being deformed came from the lower load cell. Theoretically, the lower load cell should respond about 0.1 to 0.2 msec later than the

upper load cell, i.e., the time it takes a "rod wave" to propagate the length of the specimen. Additional "start" information was provided in each test by the response of the upper load cell and by the location on the displacement plot of the backed off distance of the piston-ram (nominally 100 mils). The upper load cell occasionally showed a gradual linearly increasing load before the piston-ram could have reached it. The cause for this is not clear, and the phenomenon was not apparent in most of the tests. It may be due to an electromagnetic interaction between the Kaman displacement gage, the upper load cell, and the wires attached to each. When it did occur, the upper load cell readings were adjusted by assuming that zero load was the reading when the piston-ram began moving and that readings from the time the lower load cell registered its sharp increases were correct with respect to the zero assumed.

Figures 3.7 to 3.12 show the measured load and displacement data for the tests run at a confining pressure of 100 psi. The shapes of the load-time plots were very similar to one another but were different from the shapes obtained from the tests run with a confining pressure of 50 psi. They are very linear to about 80% of the maximum load. The maximum load is clearly discernible from the plots; it was 180-200 lbs for the slower tests and seemed to be slightly higher at 200-220 lbs for the faster tests. In some cases the load decreases slightly after it peaks while in others it holds steady at the maximum value. Comments on the 50 psi confining pressure tests regarding the discrepancies between upper and lower load cell readings and determining zeros for the load plots are relevant also to the 100 psi confining pressure tests.

Figures 3.13 to 3.18 show the measured load and displacement data for the tests run at a confining pressure of 200 psi. Again the shapes of the load-time plots are similar to one another, but different from the shapes from both the 50 psi and 100 psi confining pressure tests. They too are linear to about 80% of what one might determine as a maximum load. The maximum load, however, was either never reached prior to a specimen deformation of 15% nominal axial strain (NAS) or it occurred just prior to 15% NAS. The load increases gradually and fairly linearly from a point in the test after the sharp deviation from the initial linearity, either to 15% NAS or to a point just prior to the peak load, whichever occurs first. Comments on the 50 psi confining pressure tests regarding the discrepancies between upper and lower load cell readings and determining zeros for the load plots are relevant also to the 200 psi confining pressure tests.

It would appear that the specimen subjected to a confining pressure of 200 psi really "fails" in shear at a

point in the test much earlier than 15% NAS. The higher level of confining pressure is able to develop sufficient shear resistance on the incipient and present shear planes in the specimen so that the specimen can sustain a load that is actually higher than the load which broke down the specimen's initial grain structure. A comparable phenomenom is also evident in the tests at lower confining pressures. In the test at 100 psi confining pressure, the load mobilized after the initial grain structure failure, happened to be about the same as the load that caused the failure. In the tests at a confining pressure of 50 psi, it was less.

The load causing the collapse of the grain structure must occur during the sharp curvature of the load-time curve immediately after the initial linear portion of the curve. In the 200 psi confining pressure tests, it appears to be 275-300 pounds for the slowest tests, increasing gradually to 300-350 pounds for the fastest tests.

Examination of these twelve test curves obtained at a confining pressure of 200 psi revealed no fundamental way to determine the grain structure collapse load for the specimen. The characteristic shape of these curves, however, does suggest a systematic though somewhat arbitrary method. By extending upward the linear initial part of the load-time curve before the grain structure collapsed and extending backward the sloping somewhat linear part of the curve after the grain structure collapsed, the intersection of these straight lines gives a load which might be taken as the grain structure collapse load. The corresponding time at which it occurred can be read directly from the load-time curve at the grain structure collapse load. The displacement of the specimen top at this point can then be read from the displacement-time curve at the time just determined.

Grain structure collapse loads were determined as described above from Figures 3.13 to 3.18 for the twelve 200 psi confining pressure tests. Similar data were also read from Figures 3.1 to 3.12 for the tests with confining pressures of 50 and 100 psi. However in these tests, the data were read directly from load-time curves as the maximum load. The data are tabulated in column 9 of Table 3.1. The grain structure collapse loads are plotted as a function of the logarithm of test velocity on Figure 3.19. Though the data are scattered, it is clear that the grain structure collapse load for remolded CARES-Dry soil specimens, 0.75 inches in diameter and 1.5 inches in height and with a moisture content of 3.2% and a dry density of 118.5 pcf, increases slightly as test velocity increases from 0.003 ips to 9.0 ips when the confining pressure is 200 psi. A similar trend at lower confining pressures is not evident for the range of test velocities shown.

3.3 STRESS-STRAIN

A summary of the load-displacement data contained on Figures 3.1 to 3.18 is tabulated in columns 10-15 of Table 3.1 and plotted on Figure 3.20. The loads measured by the upper and lower load cells were averaged and the results reduced to principal stress difference (PSD) by dividing them by the specimen cross-sectional area, displacements were reduced to nominal axial strain (NAS) by dividing them by the specimen length, and then the results from identical test pairs were averaged. The values of PSD were obtained at NAS values of 0.5%, 1.0%, 2.0%, 4.0%, 8.0%, and 15.0%; these values of NAS were chosen to allow a clearer and simpler presentation of the data in aggregate. The six values chosen incorporate the linear range of stress-strain behavior (0.0 to 1.0%), the collapse of the specimen grain structure (1.0 to 4.0%), and the specimen plastic shear behavior (4.0 to 15.0%).

Detailed stress-strain data for each of the thirty-six tests are shown on Figures 3.21 to 3.23. These are plotted to 3.0% NAS to expand the curves during low levels of PSD and NAS. Figure 3.21 shows the data for the two slowest test velocities, Figure 3.22 for the two middle velocities, and Figure 3.23 for the two fastest velocities.

The effects of confining pressure on the stress-strain curves are clearly shown on Figure 3.20. With increasing confining pressure, the slopes of the initial linear part of the curves increase, the PSDs at the grain structure collapse load increase, and the plastic shear failure PSDs increase.

The test velocities for each curve on Figure 3.20 are indicated. Though Figure 3.20 does not show a strong presence of rate effects on the stress-strain behavior of the soil, it does suggest that the noticeable increases in PSD at the grain structure collapse load and during plastic shear failure occur when the test velocities and confining pressures are highest, an observation consistent with the grain structure collapse load data on Figure 3.19.

3.3 STRESS LEVEL-VELOCITY

To examine more closely the effect of test velocity on the magnitude of the PSD, Figures 3.24 to 3.26 were prepared. Figure 3.24 plots PSD against the logarithm of the test velocity, first at NAS of 0.5% and then at 1.0%. Twelve data points are shown for each confining pressure; one point was obtained for each test by averaging upper and lower load cell readings. The PSD at 0.5% and 1.0% NAS deal with the specimen before its grain structure failed. Moreover, these PSD magnitudes are proportional to the secant moduli for the

specimens at 0.5% and 1.0% NAS. To the extent that specimen stress-strain curves are linear, the PSD magnitudes are also proportional to the tangent moduli for the specimens.

Although the data are scattered on Figure 3.24, they nonetheless clearly show the effects of confining pressure on PSD or secant modulus at low stress levels -- an effect consistent with the one observed on Figure 3.20. There is no apparent effect of test velocity on PSD or secant modulus at NAS of 0.5% and 1.0%. This is most clear for the tests at a confining pressure of 200 psi where the test data are least scattered, and seems to be indicated also at the lower confining pressures. There is, however, an inconclusive suggestion that at NAS of 0.5% and 1.0% when the confining pressure was 50 psi the magnitude of PSD and corresponding secant modulus may be less at the deformation velocity of 9.0 ips than at slower velocities. Recall that at these values of NAS the grain structure has not yet broken down.

Figure 3.25 is similar to Figure 3.24 except that the values of NAS used were 2.0% and 4.0%. The PSD values at NAS of 2.0% and 4.0% deal with the specimen during the collapse of its grain structure, and consequently, show data and effects similar to those on Figure 3.19 which dealt directly with the grain structure collapse load. The effects of confining pressure and test velocity are the same as those observed on Figures 3.19 and 3.20. That is, increasing test velocity while the grain structure is collapsing increases the magnitudes of PSD when confining pressures are high, but not when they are low. There is no indication that PSD is lower at the 9.0 ips deformation velocity than at slower velocities when the confining pressure is 50 psi.

Figure 3.26 is similar to Figures 3.24 and 3.25 except that the values of NAS used were 8.0% and 15.0%. The corresponding values of PSD relate to the plastic shear failure of the specimen. Because seating errors and other initial effects are diminished at these larger NAS, the data on Figure 3.26 show only modest scatter. Trends at any of the confining pressures, if present, are clear. The effects of confining pressure and test velocity are consistent with those observed for Figure 3.20, and are more clearly shown. The rate effect observed for the grain structure collapse load would seem to occur also for the plastic shear failure of the specimen. Namely, increasing the test rate increases the shear strength of the specimen slightly when the confining pressures are high, but apparently not at all when they are low. There clearly is no decrease in the strength of the specimen at low confining pressure and high deformation velocity.

3.5 STRAIN ENERGY-VELOCITY

Another perspective of the stress-strain behavior of the test specimen may be obtained by determining the strain energy absorbed by the specimen during deformation. Strain energy density (strain energy per unit of volume) of the soil specimen is most easily calculated as the area under the stress-strain curve from the beginning of the curve to the point on the curve where the behavior is to be evaluated. Hence the strain energy density contains directly the effects of the shape of the specimen's stress-strain curve from its beginning to the point of evaluation.

Figures 3.27 to 3.29 are plots of strain energy density as a function of the logarithm of test velocity. They are parallel in design to Figures 3.24 to 3.26 just discussed. The effects of confining pressure and test velocity on strain energy density that can be discerned from Figures 3.27 to 3.29 are the same as the effects on stress level and modulus already noted on Figures 3.24 to 3.26. Figure 3.27 shows a suggestion of a decrease in strain energy density with high deformation velocity when the NAS is low (0.5% and 1.0%) and the confining pressure is low (50 psi). The scatter and paucity of the data, however, prevent a conclusive determination of this effect just as it did on Figure 3.24.

3.6 STRENGTH ENVELOPES

An examination of the test results on the CARES-Dry soil in terms of the Mohr-Coulomb failure criterion is instructive. When the specimen is at failure, according to Mohr-Coulomb, the Mohr's circle for its state of stress is tangent to the Coulomb failure envelope. The equation of the envelope is:

$$s = c + \sigma_n \tan\phi \qquad \text{where}$$

s - shear strength of the soil and the shear stress on the plane of failure,
c - cohesion intercept,
σ_n - normal stress on the plane of failure,
ϕ - angle of internal friction, $\tan\phi$ is the slope of the envelope.

Another more conveniently developed envelope from triaxial shear data is a plot of the maximum shear stress (or one-half PSD) at failure versus the average principal stress (or one-half the sum of the confining pressure and the nominal axial stress at failure). The equation for this envelope is:

$$\tau_{max} = d + p_{avg} \tan\beta \qquad \text{where}$$

τ_{max} - maximum shear stress in the specimen, = PSD/2,

d - intercept,

p_{avg} - average principal stress in the specimen, = CP+PSD/2,

β - angle of the envelope
tanβ is the slope of the envelope

These stresses (τ_{max} and p_{avg}) occur on a plane inclined at 45° from the axis of the specimen whereas the plane of failure of the Coulomb stresses is inclined at an angle of 45°-ϕ/2 from the specimen axis. If the Coulomb envelope is a straight line, so is the plot of maximum shear stress versus average principal stress. The two envelopes are related as follows:

$$\sin\phi = \tan\beta$$
$$d = c\cos\phi$$
$$s = \tau_{max}\cos\phi$$
$$\sigma_n = p_{avg} - \tau_{max}\sin\phi$$

Figure 3.30 shows the plots of maximum shear stress versus average principal stress for specimens deformed to 4.0% and 15.0% NAS. At 4.0% NAS the collapse of the grain structure was just complete and at 15.0% NAS the specimens had deformed considerably in plastic shear. Each data point on the plots are the average of the results from the corresponding identical test pair. The eighteen data points for each plot reflect all six test velocities. A linear regression was used to determine the values for parameters d and β; the associated values of the Coulomb parameters (c and ϕ) were then calculated using the relations shown above. The values of both sets of parameters are shown on the figure.

The linearity of both plots is excellent as shown by their coefficients of variation (0.995 and 0.999). At NAS of 15.0%, the value of c is less and ϕ is greater than they are at NAS of 4.0%. Recall that the load on specimens subjected to a confining pressure of 50 psi decreased after 4.0% NAS was reached but increased for specimens subjected to a confining pressure of 200 psi.

All test velocities plot close to the same envelope, suggesting that, for the test moisture content (3.2%) and dry density (118.5 pcf), one set of Coulomb strength parameters applies for the CARES-Dry soil at a particular NAS after grain structure collapse and within the range of test velocities and confining pressures used in this test series. The small increase in PSD at 4-15% NAS observed at high deformation velocity (9.0 ips) and confining pressure

(200 psi) and shown on the stress level and strain energy versus deformation velocity plots (Figures 3.25, 3.26, 3.28, and 3.29) do not show on the strength envelopes. The increased load due to rate is reflected only in the axial stress on the specimen, and therefore increases equally both the maximum shear stress and the average principal stress in the specimen. Within the experimental accuracy of the test results, these increases track close to the strength envelopes.

TABLE 3.1

SUMMARY of SPECIMEN DATA, TEST PARAMETERS, and TEST RESULTS

Test	Height (in)	Diameter (in)	Moisture Content (%)	Dry Density (pcf)	Confining Pressure (psi)	Nominal Duration (msec)	Piston Velocity (ips)	Grain Structure Collapse Load (lbs)	PSD at selected values of NAS					
									NAS 1/2% (psi)	NAS 1% (psi)	NAS 2% (psi)	NAS 4% (psi)	NAS 8% (psi)	NAS 15% (psi)
X31	1.496	0.756	3.2	119	50	80000	0.0049	140	100	230	305	293	275	267
X34	1.488	0.755	3.1	119	50	80000	0.0044	140	105	240	310	304	286	266
X32	1.508	0.754	3.4	118	100	80000	0.0045	170	120	250	380	425	425	432
X35	1.500	0.755	3.1	119	100	80000	0.0035	180	195	320	400	423	432	439
X33	1.498	0.755	3.1	118	200	80000	0.0034	285	230	400	560	628	681	737
X36	1.503	0.755	3.3	118	200	80000	0.0033	305	310	480	595	660	717	739
X39	1.507	0.756	3.1	118	50	2000	0.16	135	120	260	295	271	246	231
X41	1.507	0.755	3.1	118	50	2000	0.16	140	140	255	305	284	253	232
X10	1.492	0.754	3.2	120	100	2000	0.12	200	50	170	400	455	422	395
X12	1.495	0.754	3.4	120	100	2000	0.14	195	175	340	430	441	415	408
X38	1.504	0.755	3.1	118	200	2000	0.16	310	270	465	610	692	763	782
X42	1.496	0.755	3.2	119	200	2000	0.15	310	310	485	610	685	737	763
X18	1.503	0.756	3.1	118	50	900	0.31	140	60	170	305	285	249	246
X37	1.502	0.755	3.1	119	50	900	0.37	145	160	290	310	296	256	238
X11	1.497	0.751	3.3	120	100	900	0.33	210	45	130	435	475	457	444
X15	1.496	0.757	3.5	118	100	900	0.31	180	195	330	395	410	409	408
X16	1.492	0.756	3.5	119	200	900	0.24	290	220	390	530	661	692	726
X17	1.508	0.754	3.1	118	200	900	0.28	285	240	470	610	617	691	734
X29	1.500	0.756	3.2	119	50	250	1.07	155	120	260	340	327	285	258
X30	1.503	0.753	3.2	118	50	250	1.09	135	150	250	300	292	264	253
X19	1.514	0.755	3.0	117	100	250	1.07	175	90	250	380	393	385	379
X27	1.500	0.755	3.1	118	100	250	1.04	200	150	300	440	454	434	417
X20	1.503	0.755	3.3	118	200	250	0.84	290	290	430	555	631	698	737
X28	1.490	0.756	3.1	119	200	250	0.85	340	250	490	680	769	811	807
X21	1.495	0.755	3.1	119	50	100	2.3	140	180	260	295	283	267	251
X24	1.496	0.756	3.1	119	50	150	1.5	150	190	300	340	310	253	261
X22	1.497	0.757	3.2	118	100	100	2.3	220	180	340	470	485	457	430
X25	1.509	0.755	3.1	118	100	100	2.5	210	60	185	440	476	465	467
X23	1.510	0.756	3.0	117	200	100	2.6	320	185	340	555	682	740	749
X26	1.495	0.754	3.3	119	200	100	2.4	330	160	420	650	735	788	809
X48	1.499	0.756	3.1	118	50	25	9.3	160	60	190	340	349	313	288
X49	1.515	0.756	3.1	118	50	25	8.6	140	80	160	305			
X43	1.504	0.754	3.3	119	100	25	9.2	215	170	320	440	482	452	405
X46	1.505	0.756	3.1	118	100	25	9.5	220	130	260	440	497	503	492
X44	1.503	0.755	3.2	119	200	25	9.2	340	265	465	725	746	794	818
X47	1.501	0.756	3.1	118	200	25	8.9	360	260	450	650	820	862	870
Avg	1.501	0.755	3.18	118.5										
Std Dev	0.006	0.001	0.12	0.7										

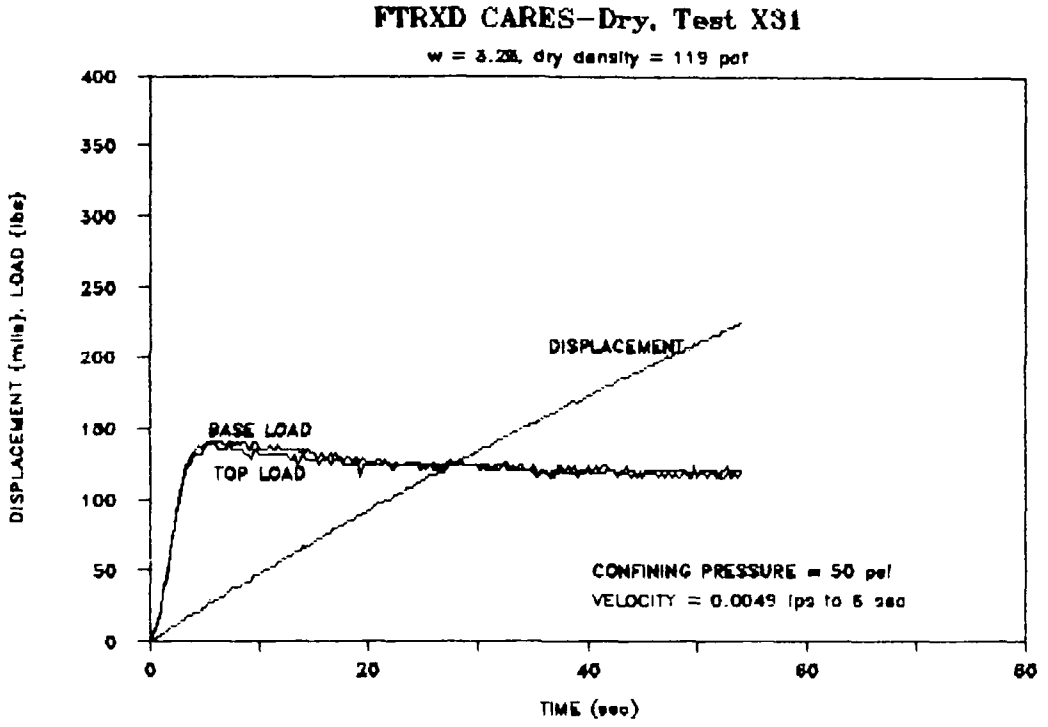

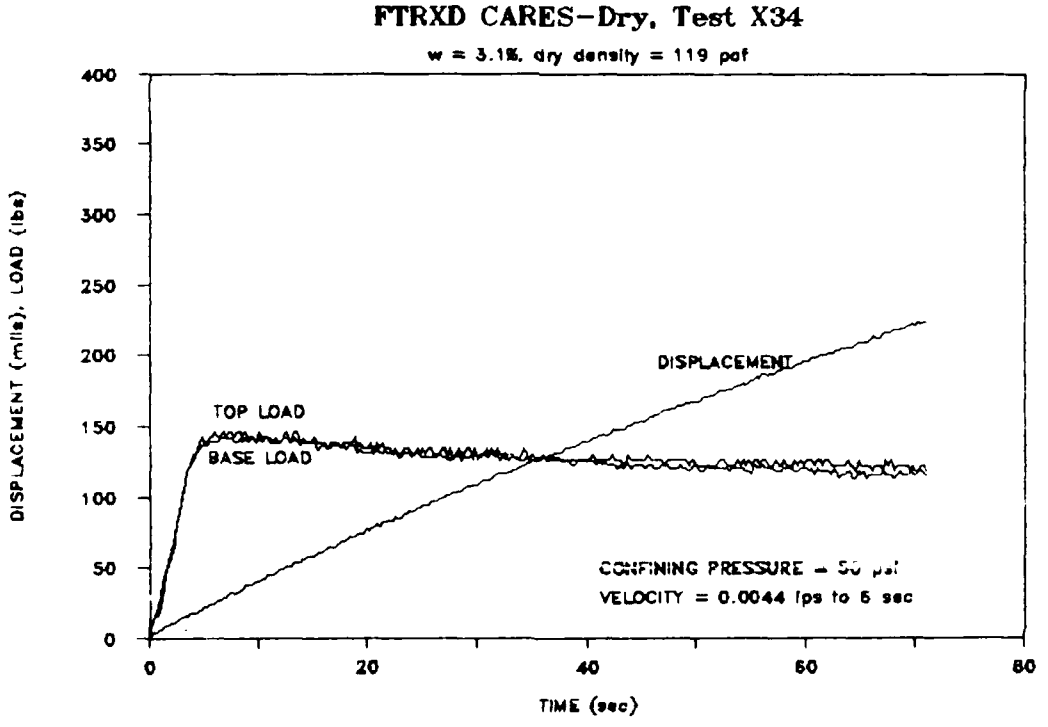

Figure 3.1, LOAD-DISPLACEMENT-TIME
(CP = 50 psi; VEL = 0.0049 and 0.0044 ips)

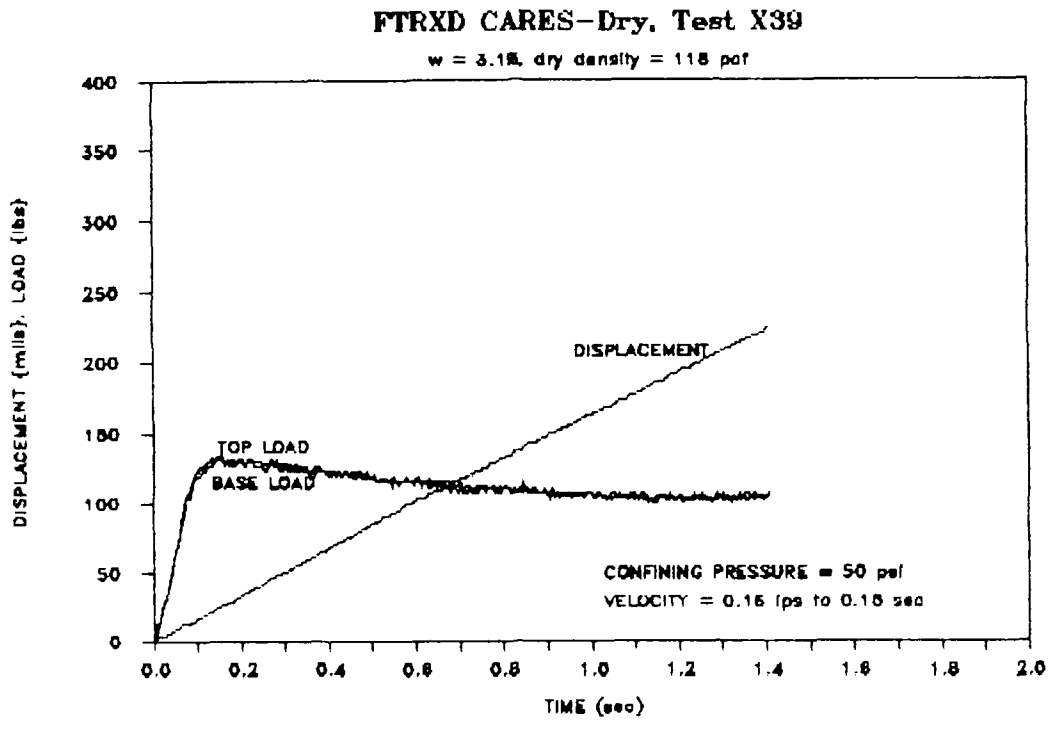

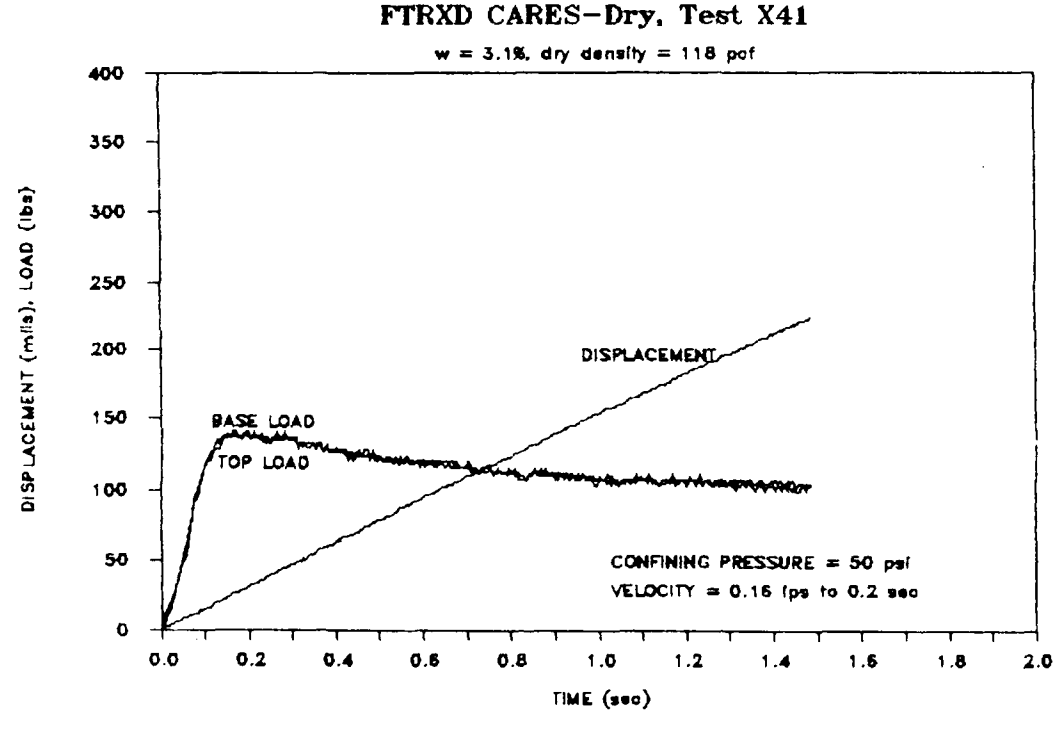

Figure 3.2, LOAD-DISPLACEMENT-TIME
(CP = 50 psi; VEL = 0.16 ips)

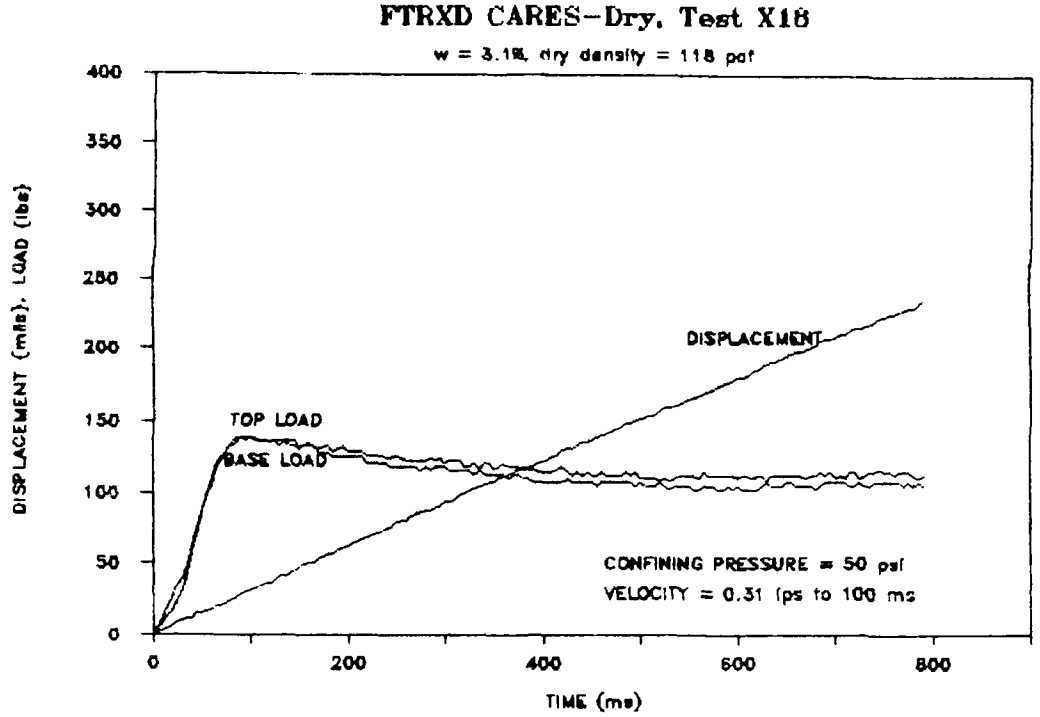

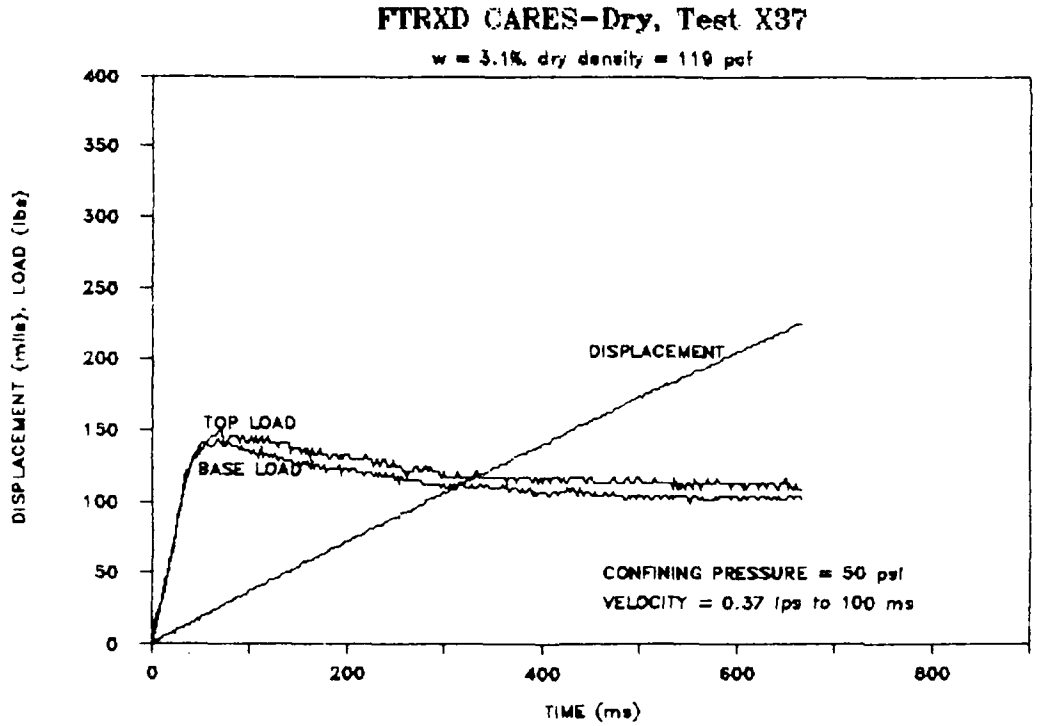

Figure 3.3, LOAD-DISPLACEMENT-TIME
(CP = 50 psi; VEL = 0.31 and 0.37 ips)

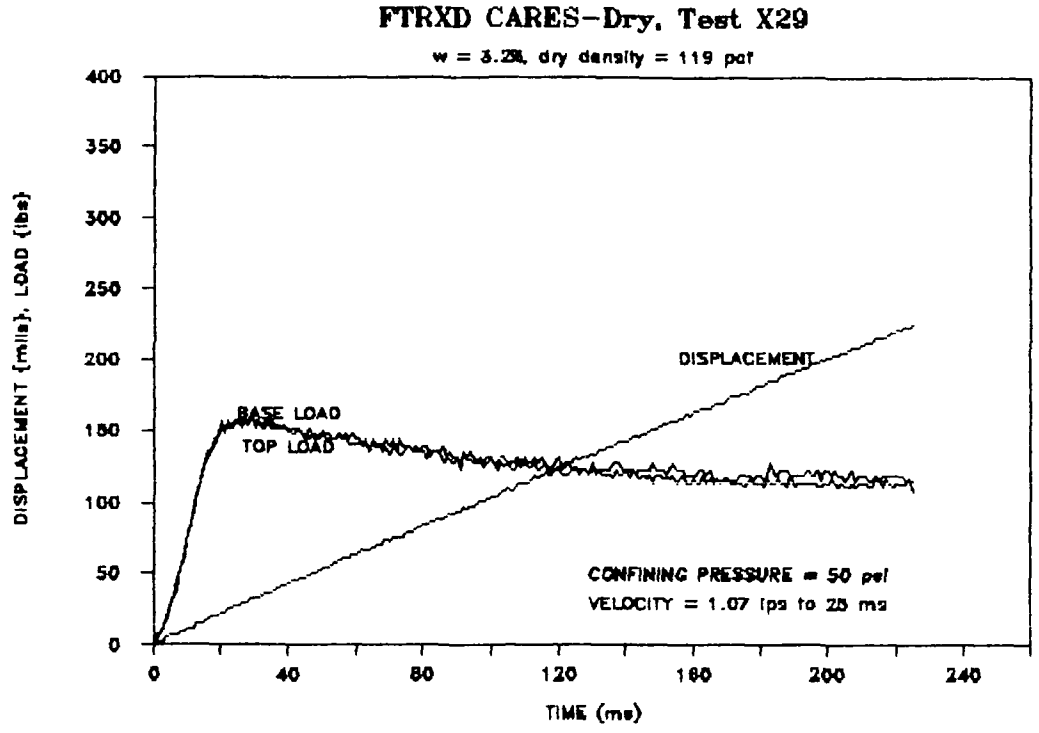

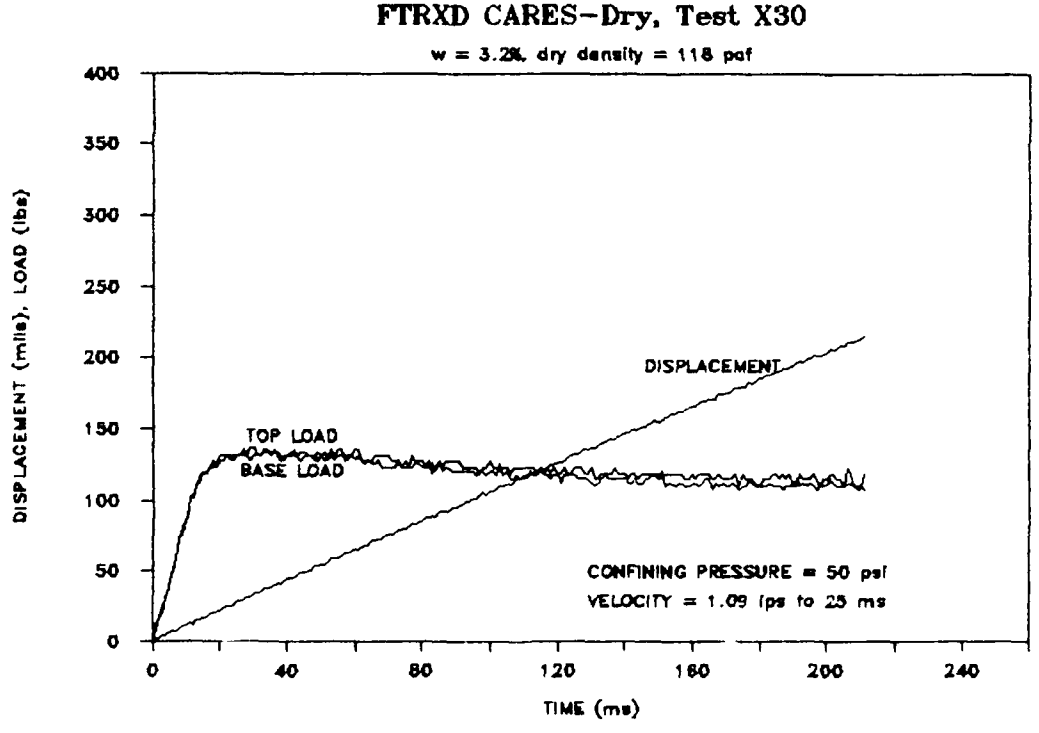

Figure 3.4, LOAD-DISPLACEMENT-TIME
(CP = 50 psi; VEL = 1.07 and 1.09 ips)

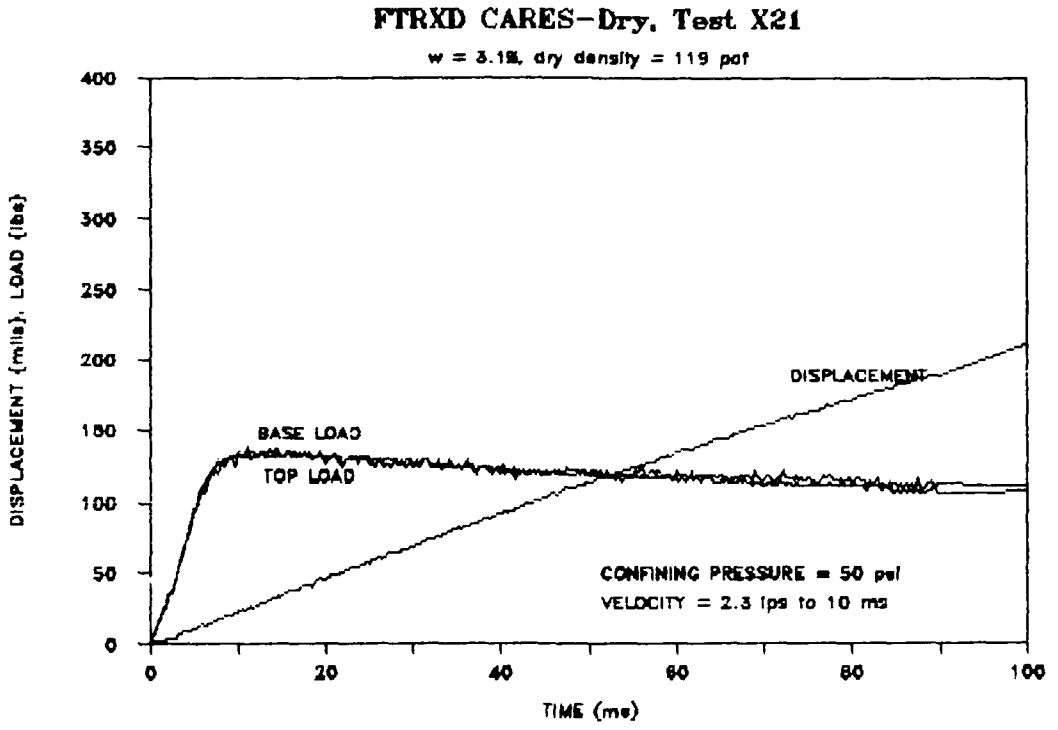

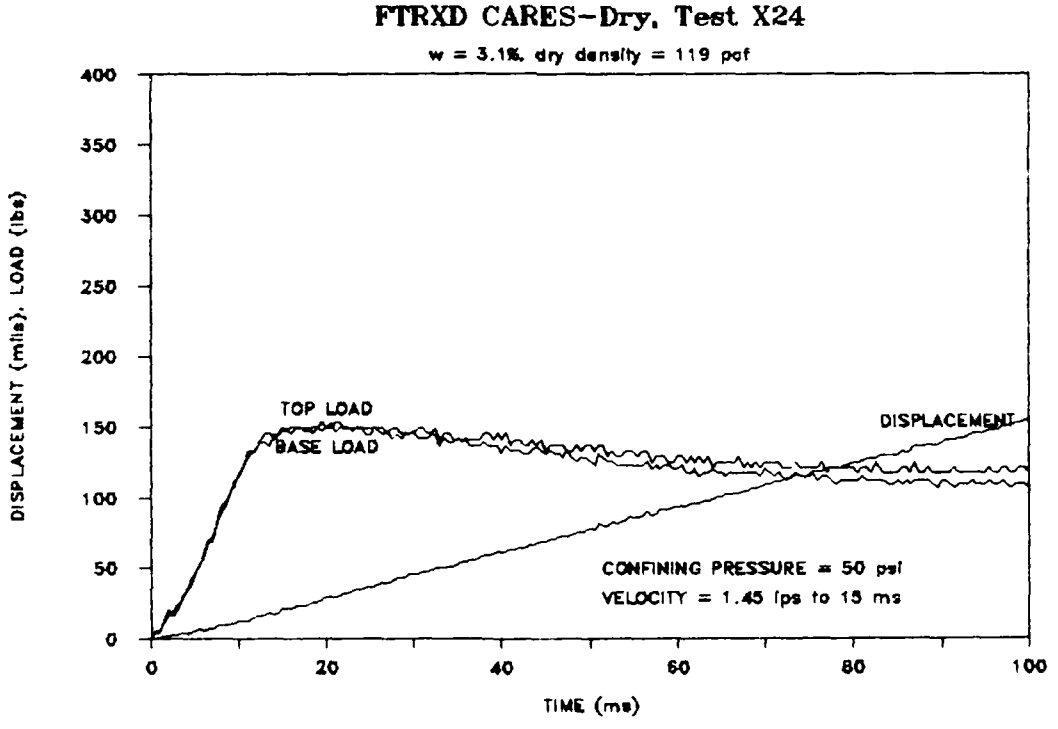

Figure 3.5, LOAD-DISPLACEMENT-TIME
(CP = 50 psi; VEL = 2.3 and 1.5 ips)

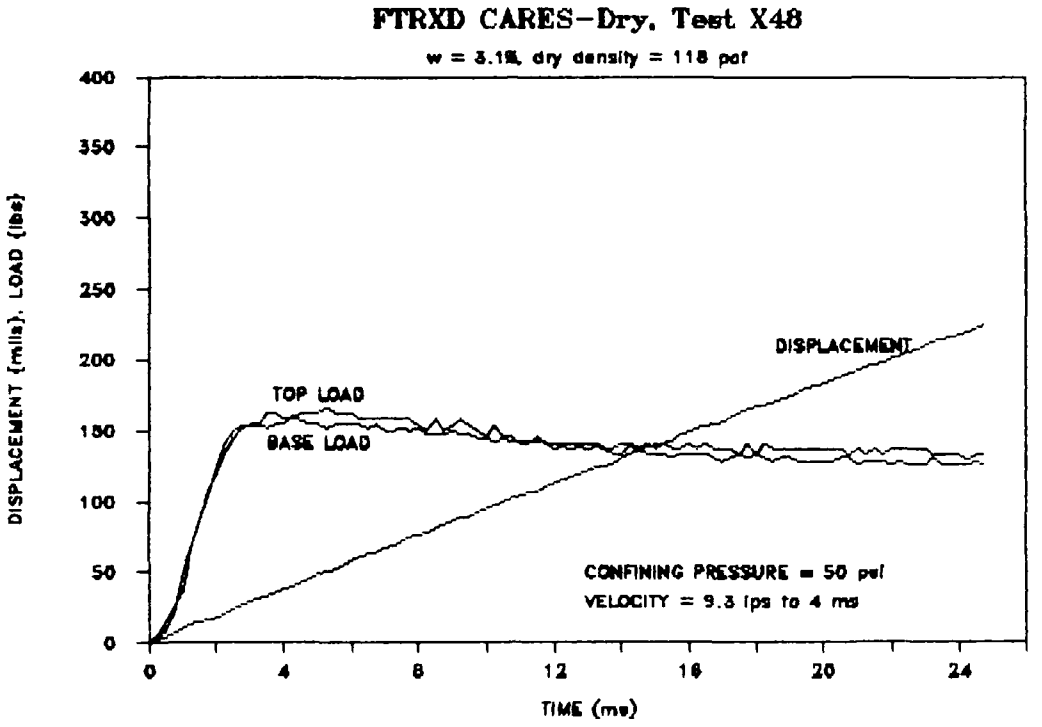

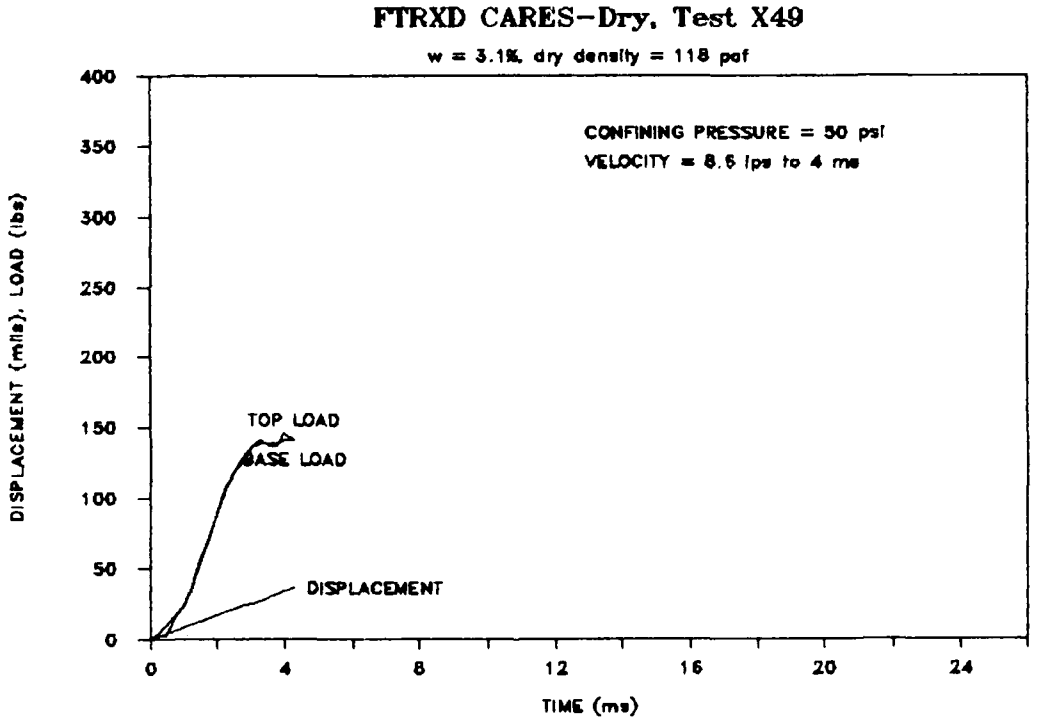

Figure 3.6, LOAD-DISPLACEMENT-TIME
(CP = 50 psi; VEL = 9.3 and 8.6 ips)

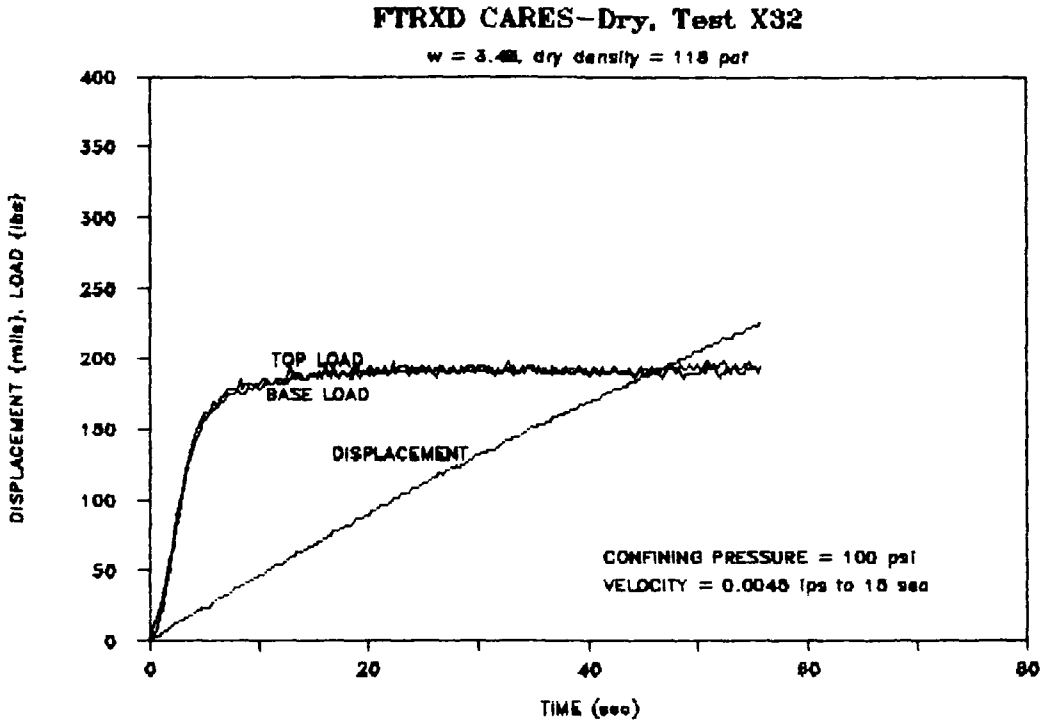

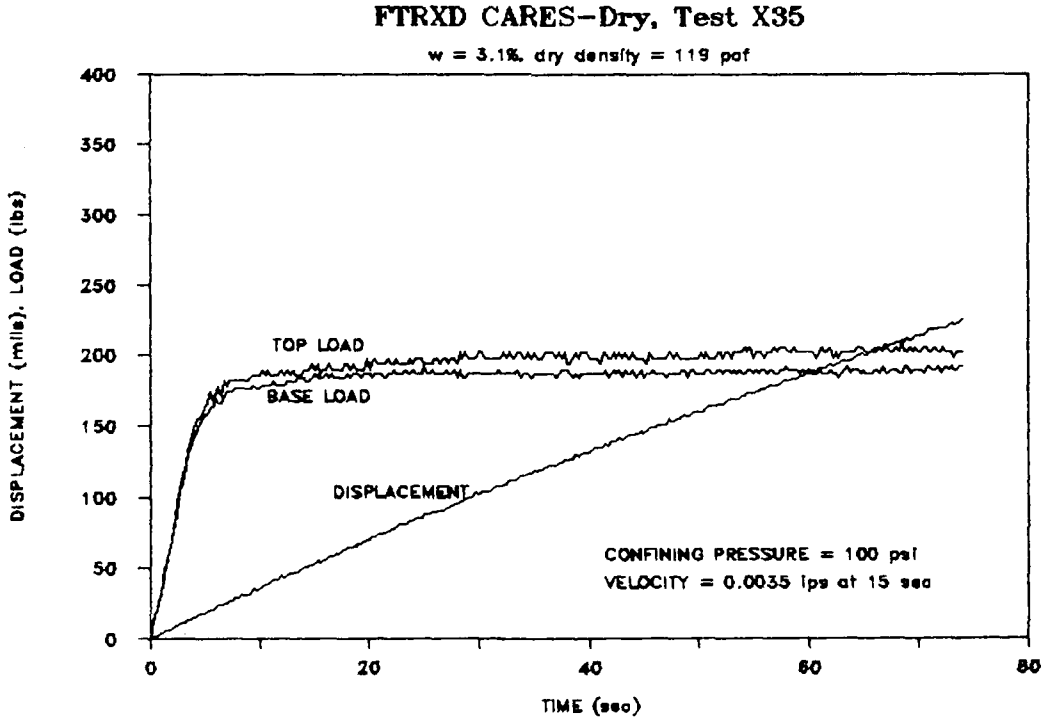

Figure 3.7, LOAD-DISPLACEMENT-TIME
(CP = 100 psi; VEL = 0.0045 and 0.0035 ips)

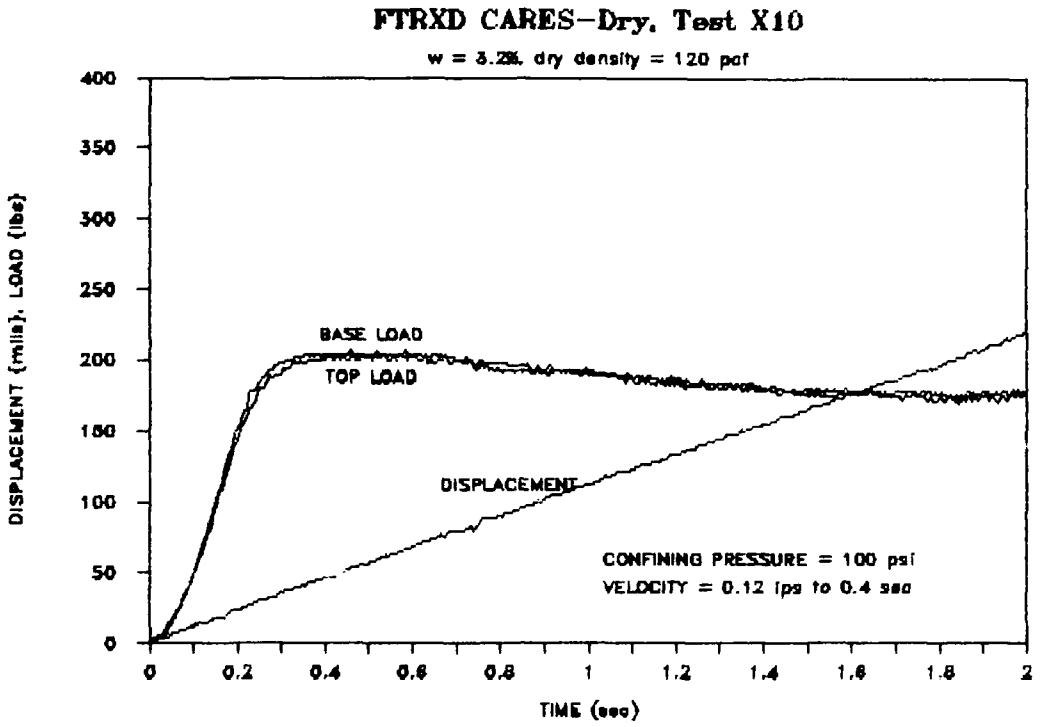

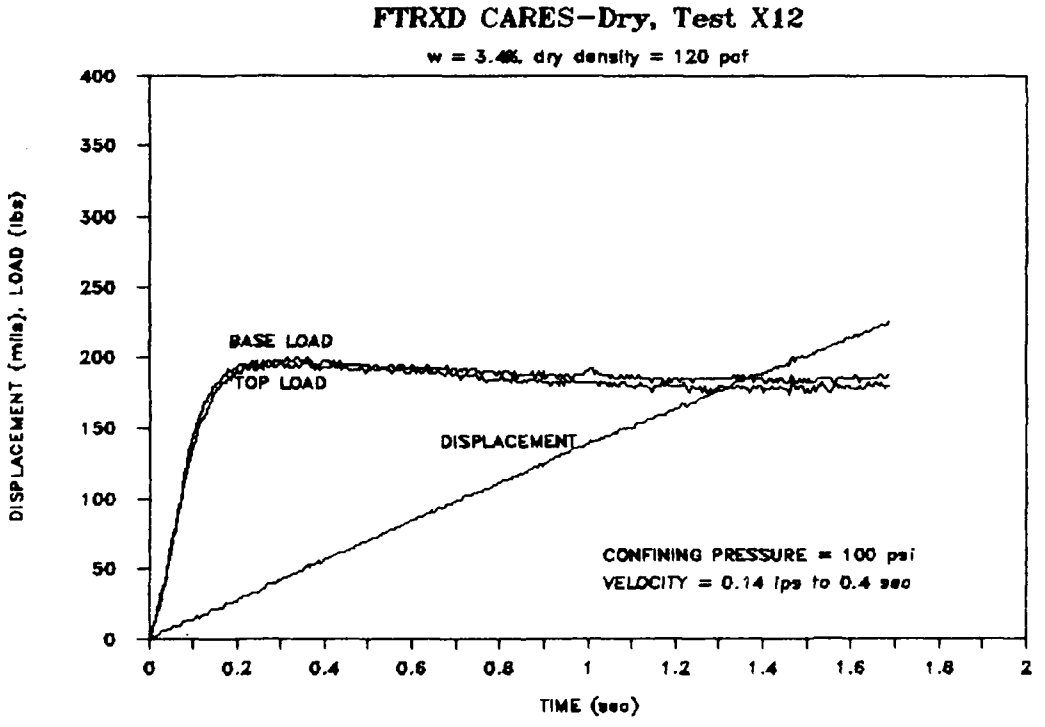

Figure 3.8, LOAD-DISPLACEMENT-TIME
(CP = 100 psi; VEL = 0.12 and 0.14 ips)

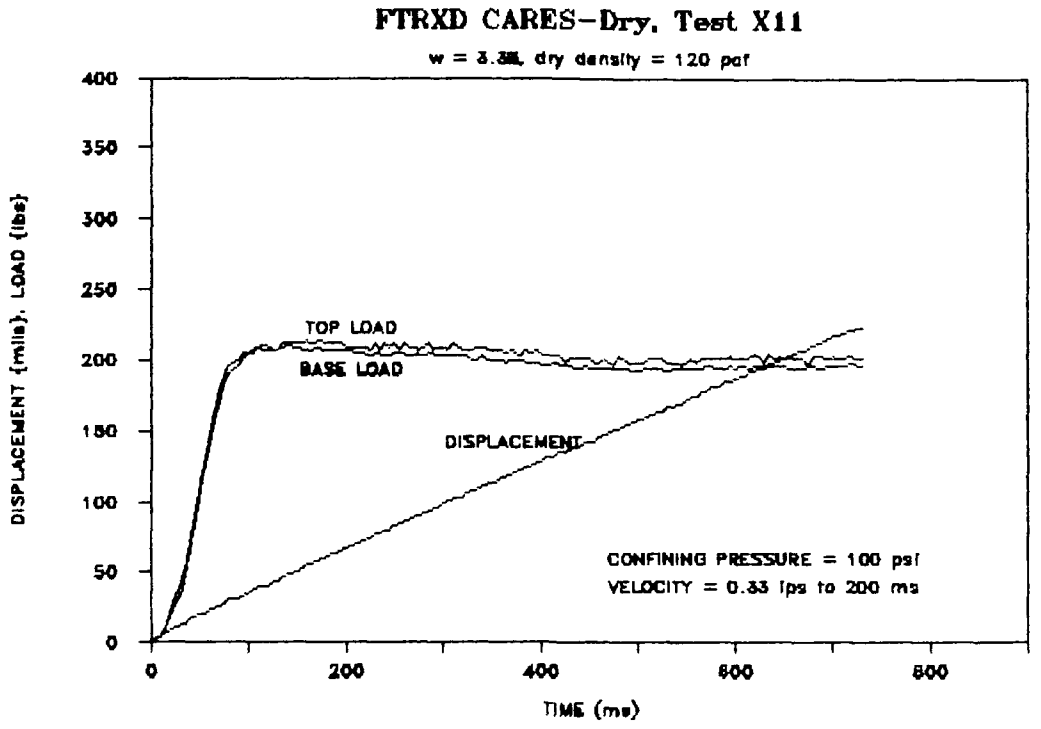

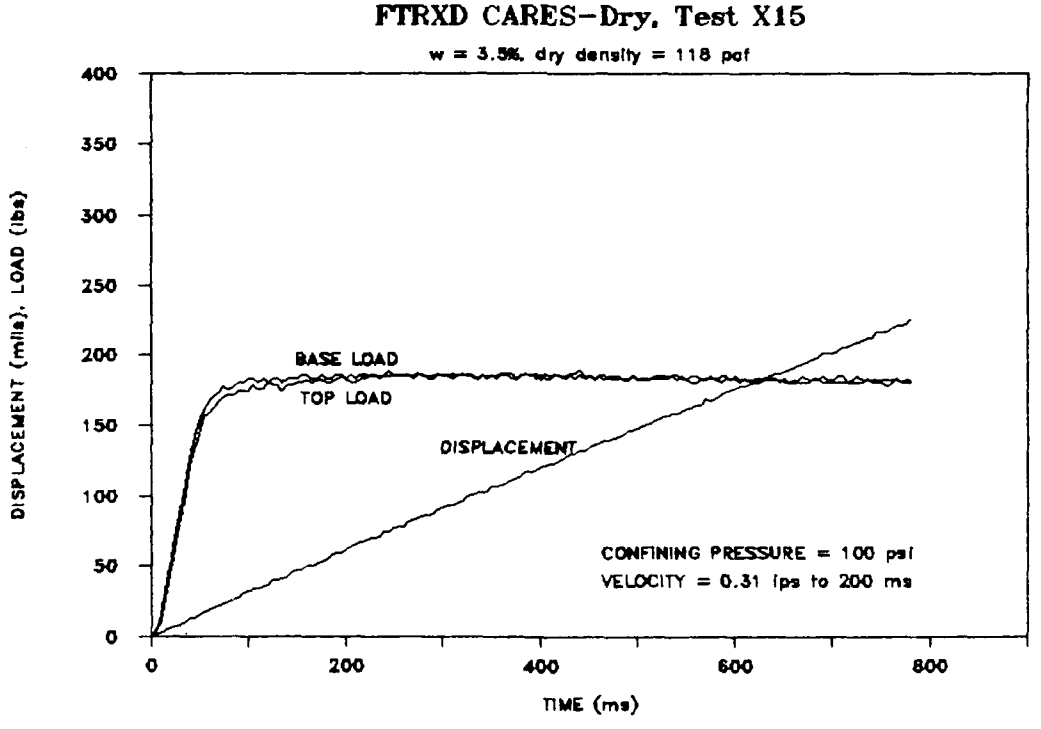

Figure 3.9, LOAD-DISPLACEMENT-TIME
(CP = 100 psi; VEL = 0.33 and 0.31 ips)

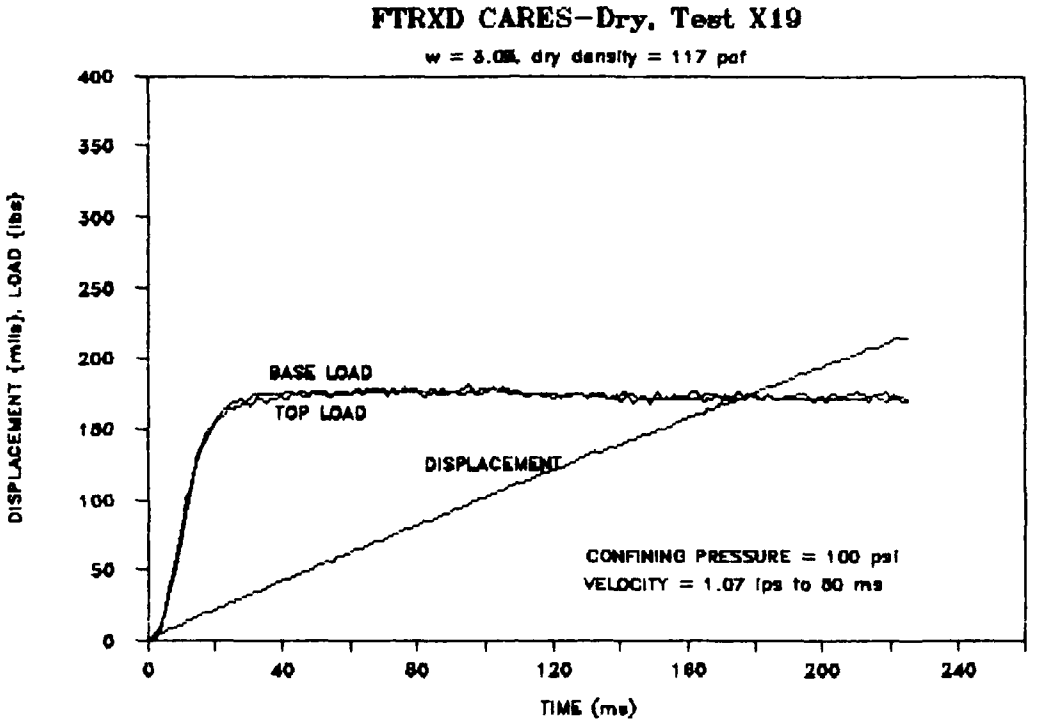

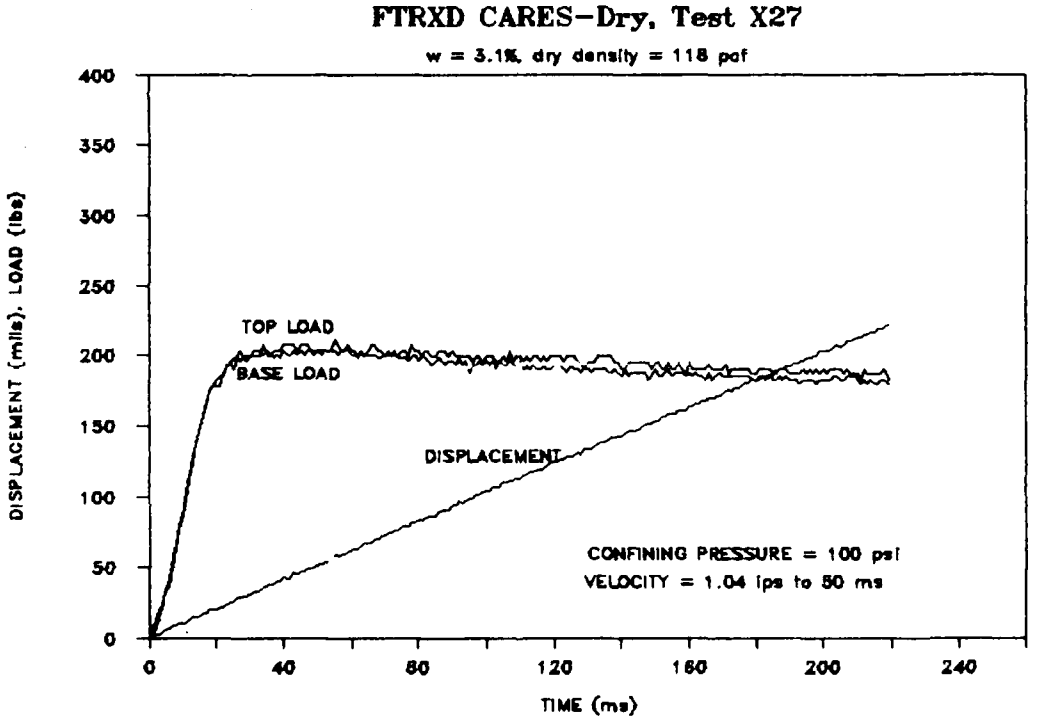

Figure 3.10. LOAD-DISPLACEMENT-TIME
(CP = 100 psi; VEL = 1.07 and 1.04 ips)

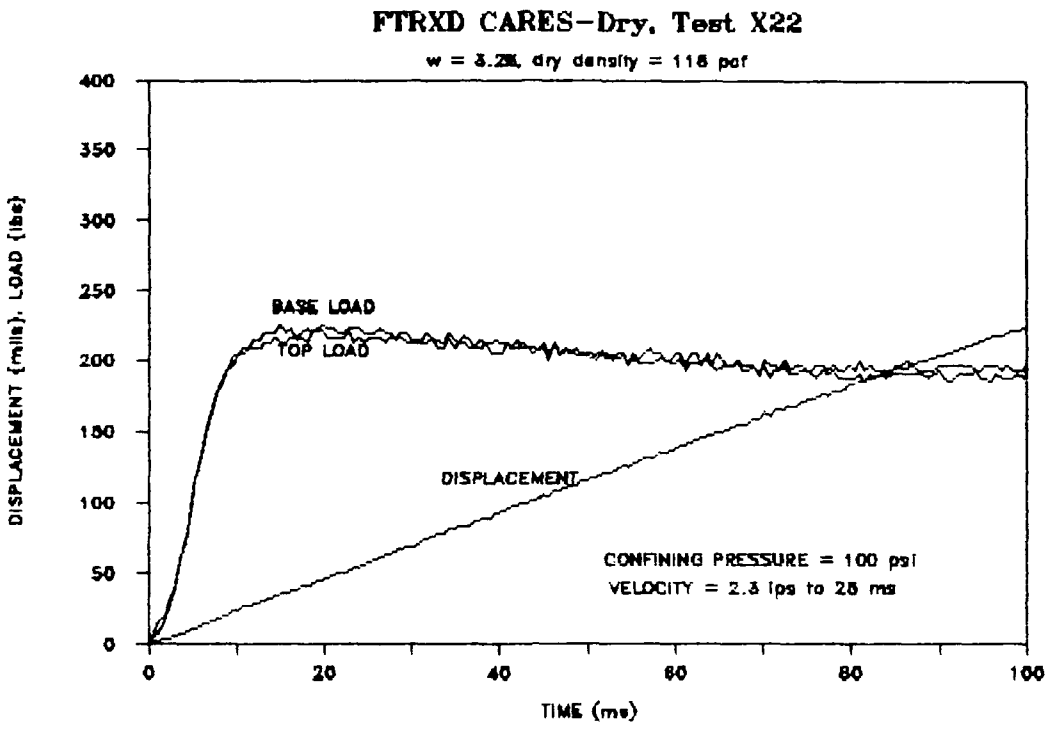

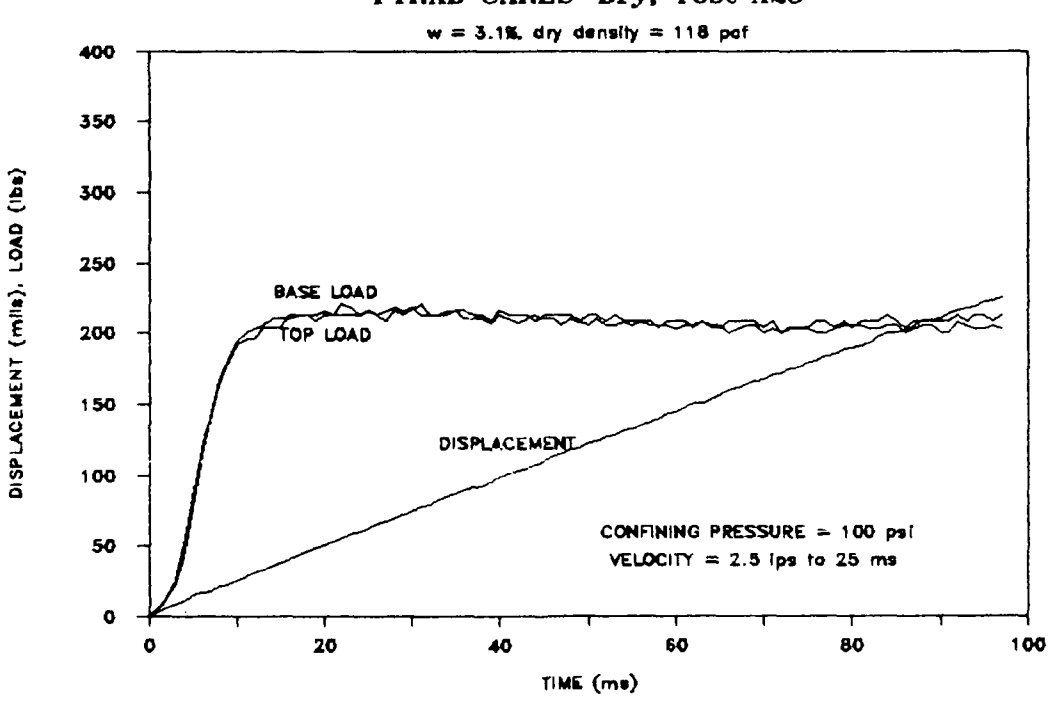

Figure 3.11, LOAD-DISPLACEMENT-TIME
(CP = 100 psi; VEL = 2.3 and 2.5 ips)

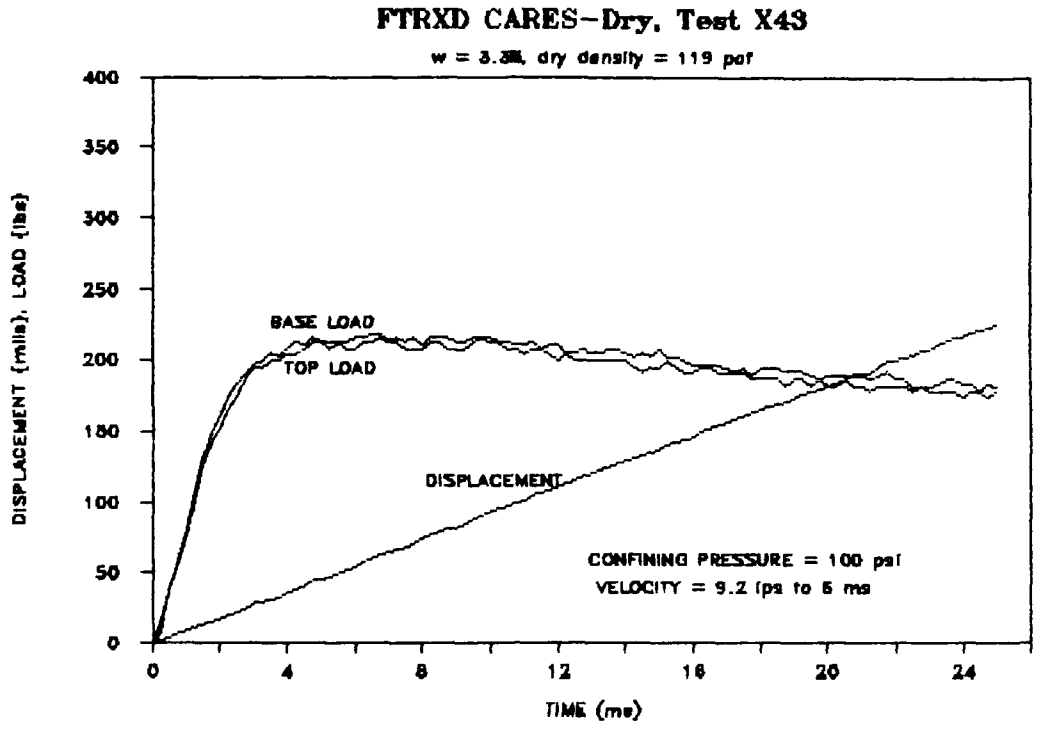

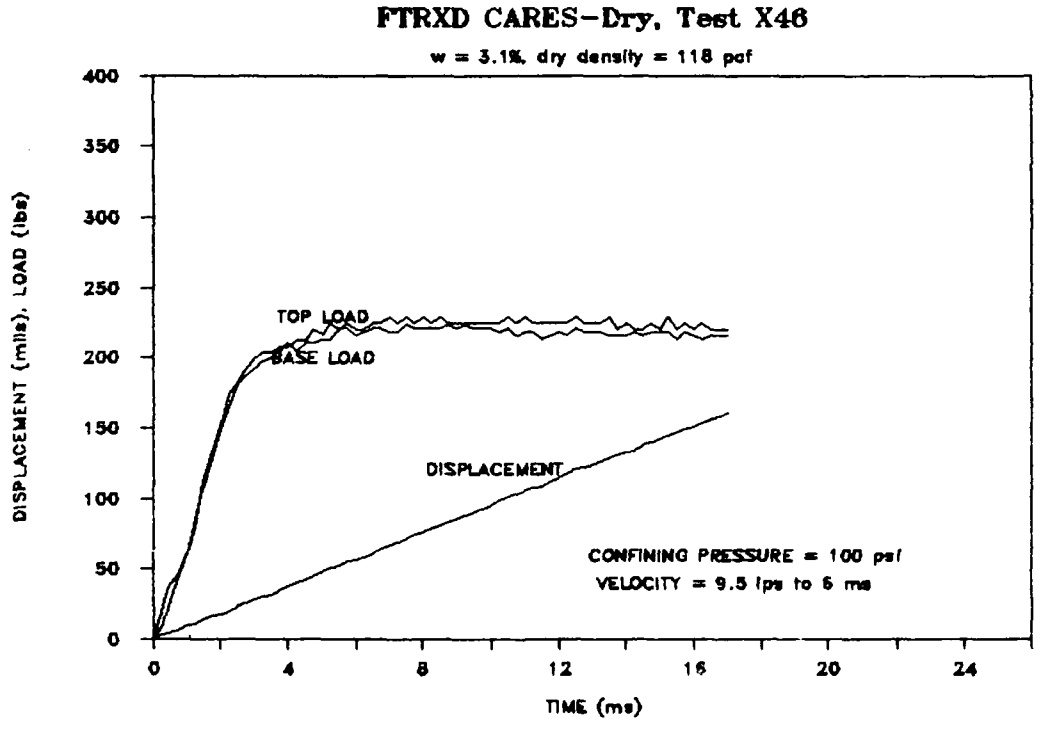

Figure 3.12, LOAD-DISPLACEMENT-TIME
(CP = 100 psi; VEL = 9.2 and 9.5 ips)

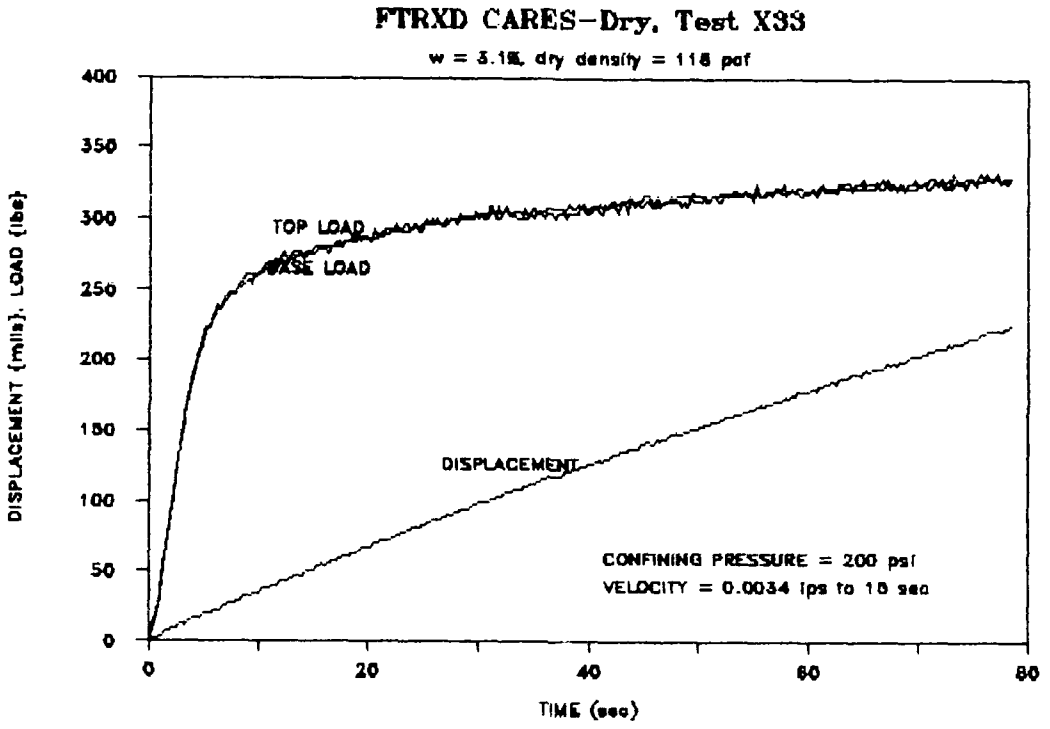

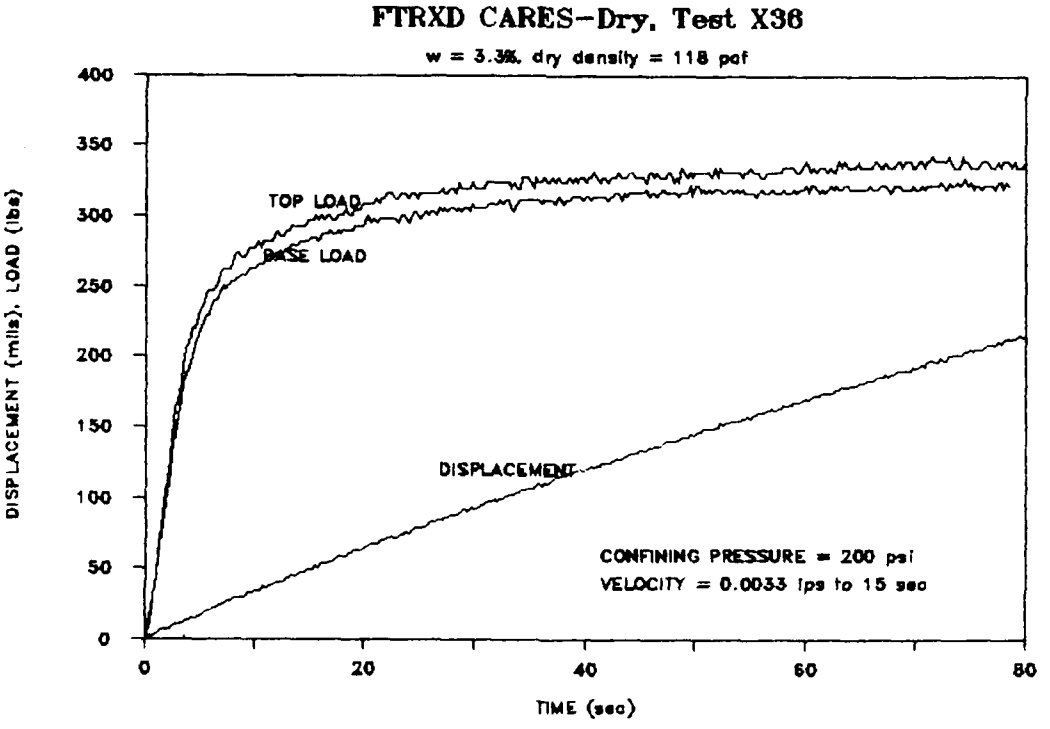

Figure 3.13, LOAD-DISPLACEMENT-TIME
(CP = 200 psi; VEL = 0.0034 and 0.0033 ips)

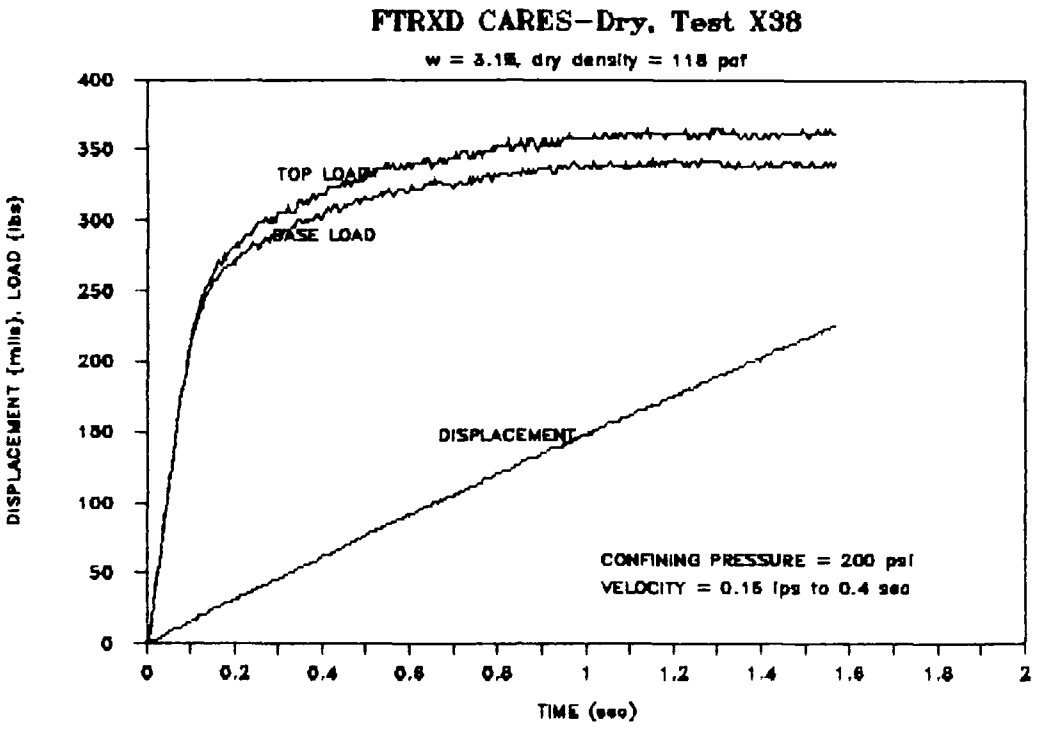

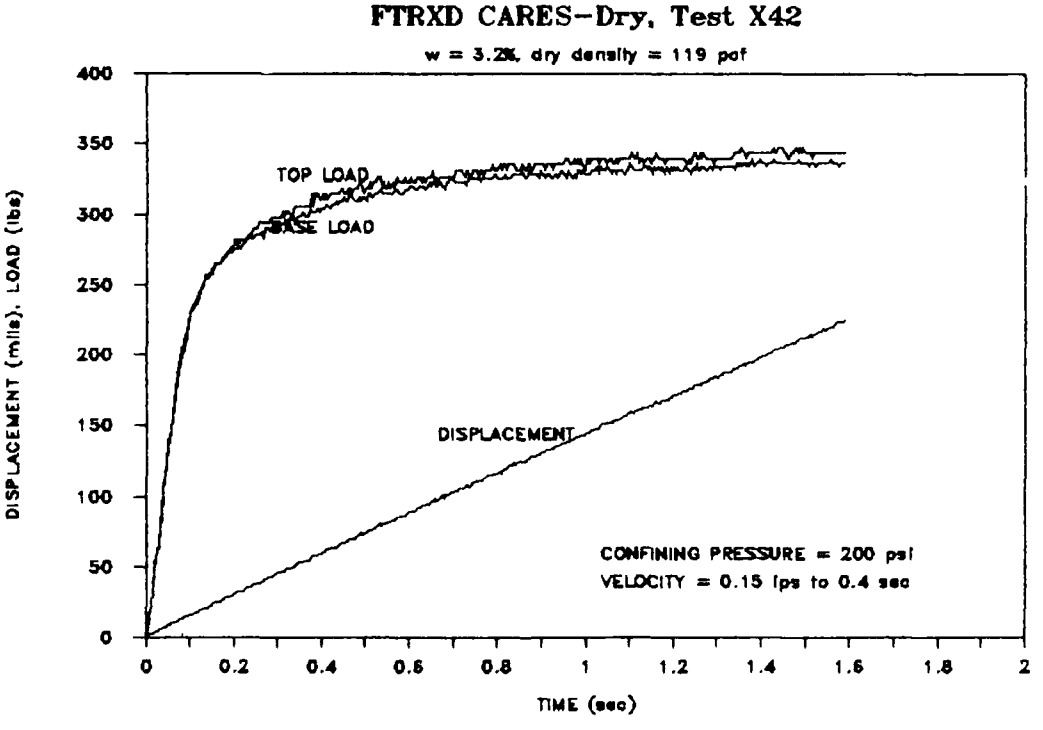

Figure 3.14, LOAD-DISPLACEMENT-TIME
(CP = 200 psi; VEL = 0.16 and 0.15 ips)

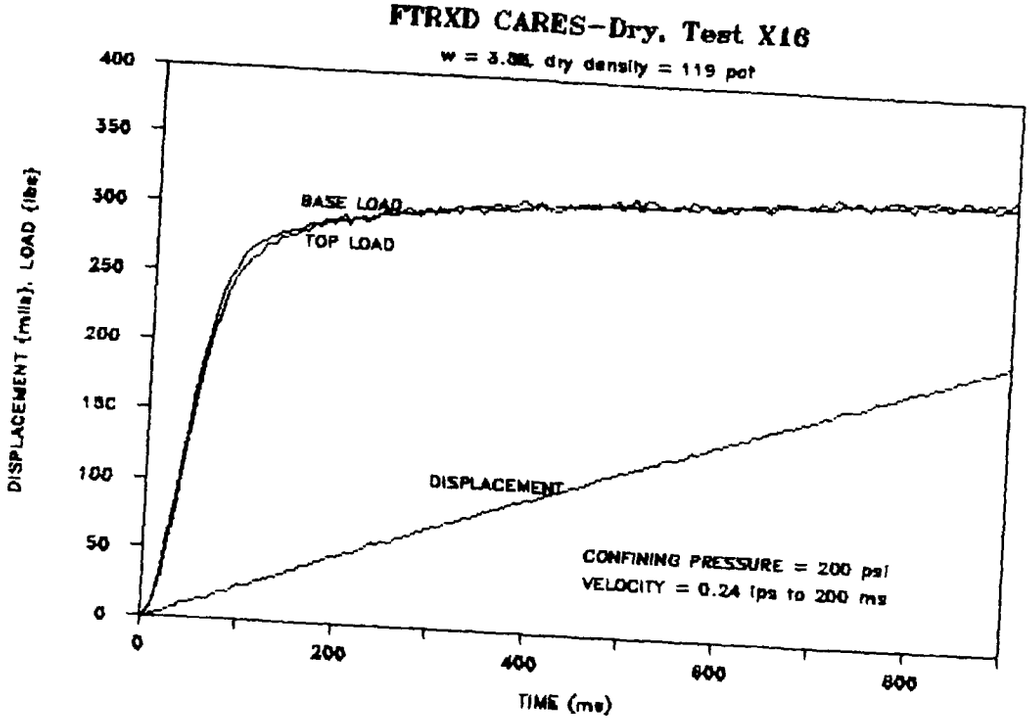

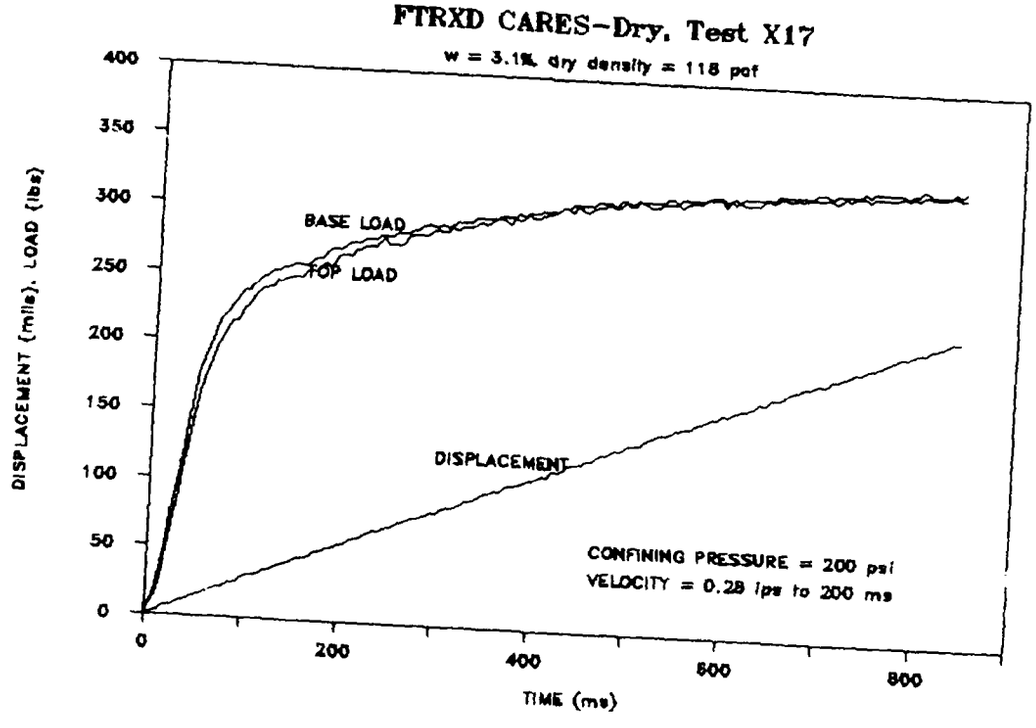

Figure 3.15, LOAD-DISPLACEMENT-TIME
(CP = 200 psi; VEL = 0.24 and 0.28 ips)

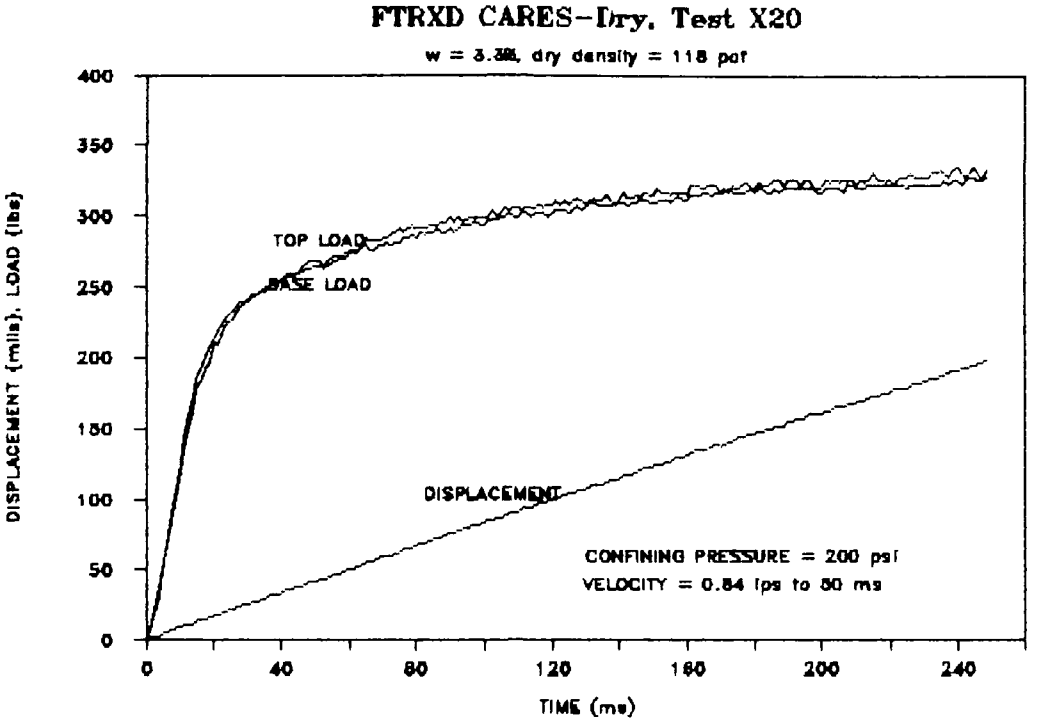

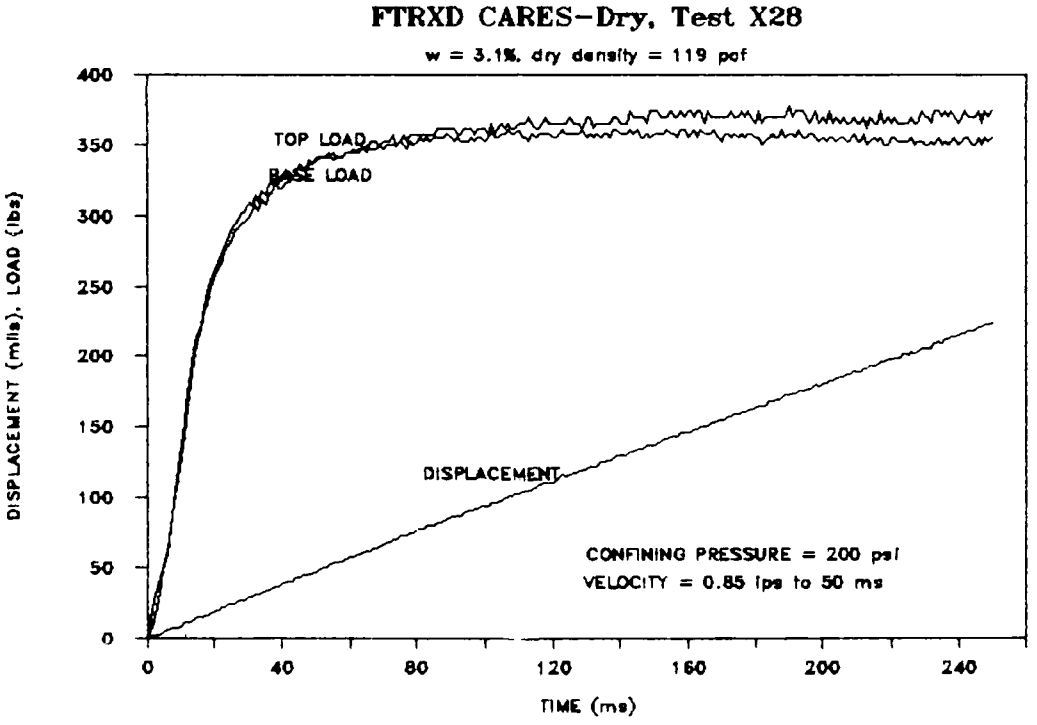

Figure 3.16, LOAD-DISPLACEMENT-TIME
(CP = 200 psi; VEL = 0.84 and 0.85 ips)

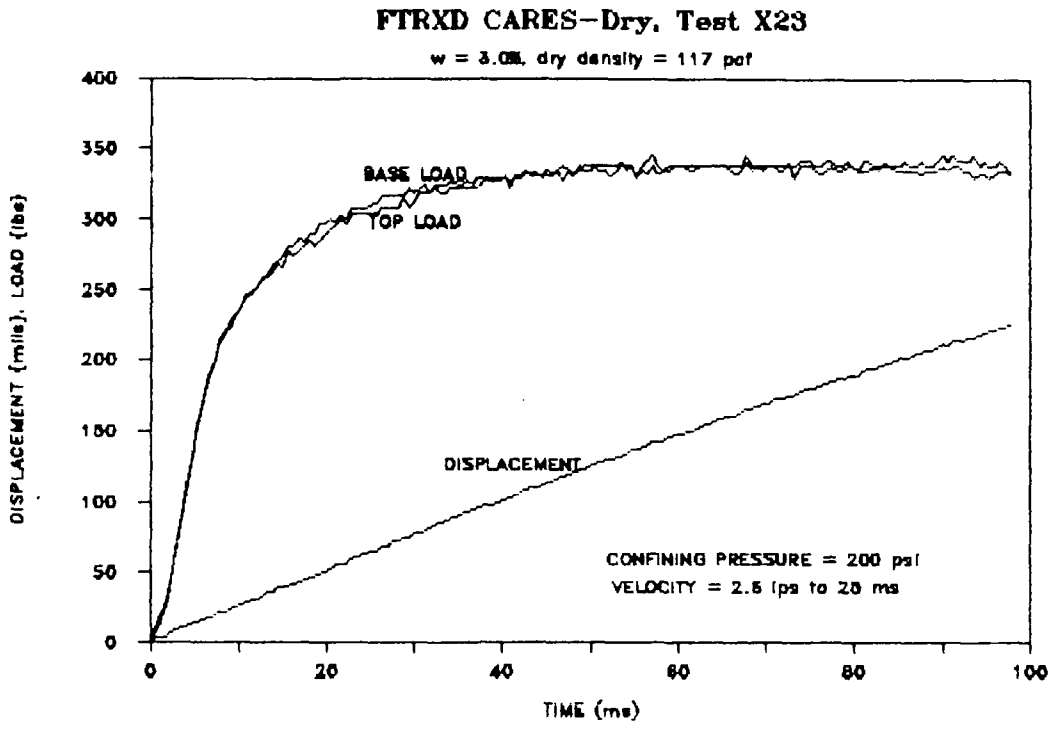

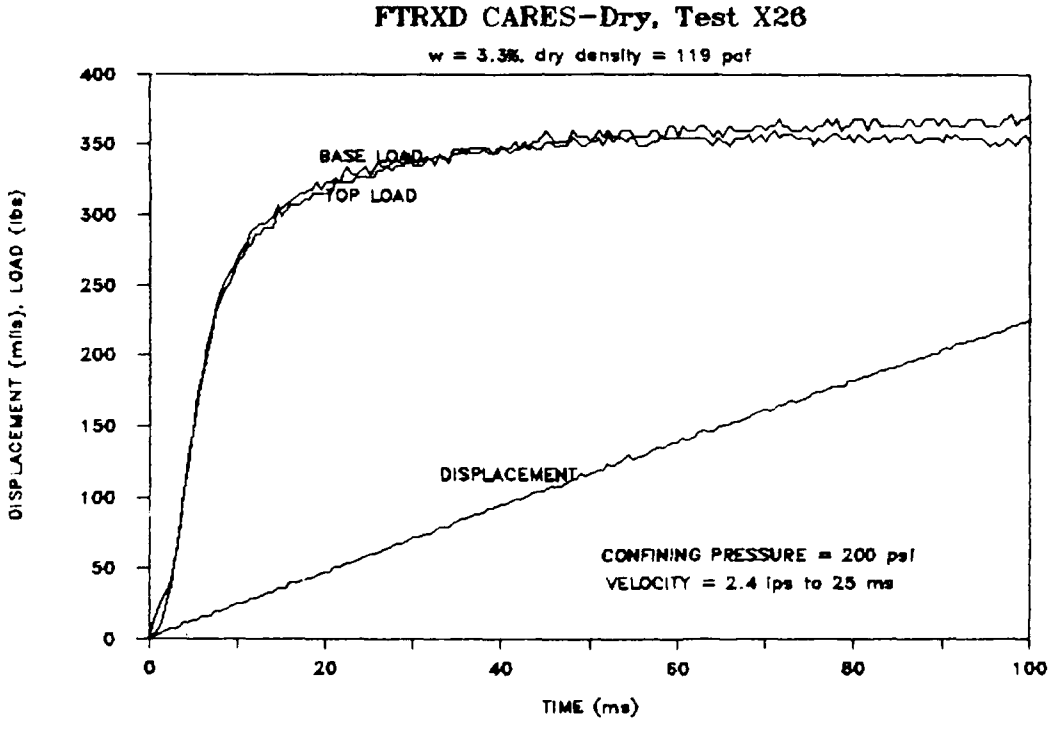

Figure 3.17, LOAD-DISPLACEMENT-TIME
(CP = 200 psi; VEL = 2.6 and 2.4 ips)

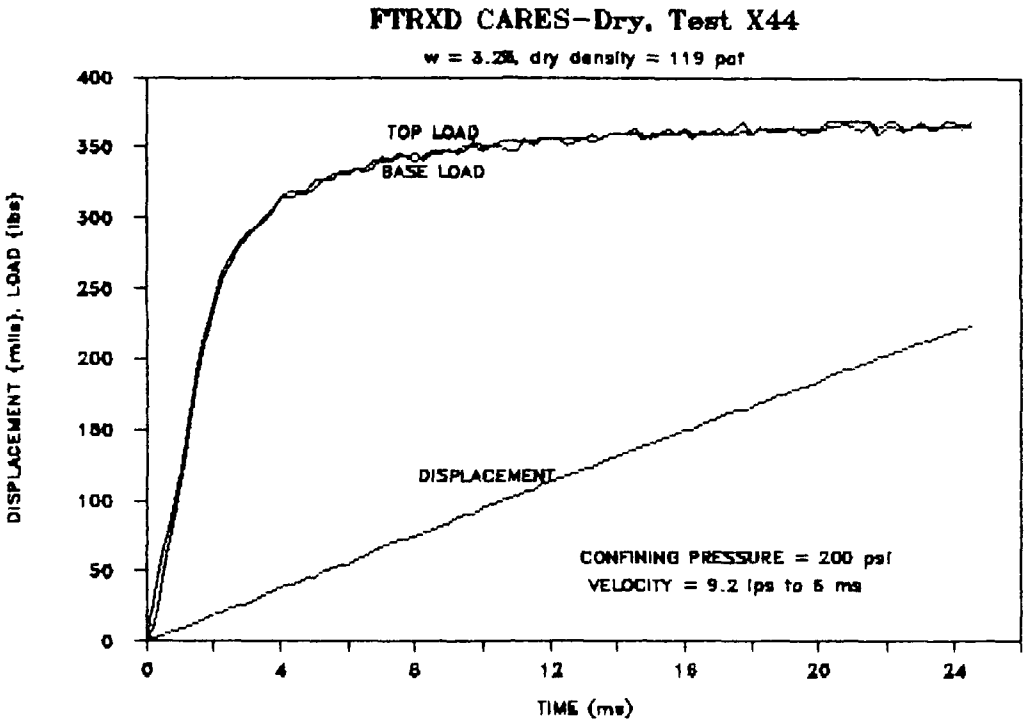

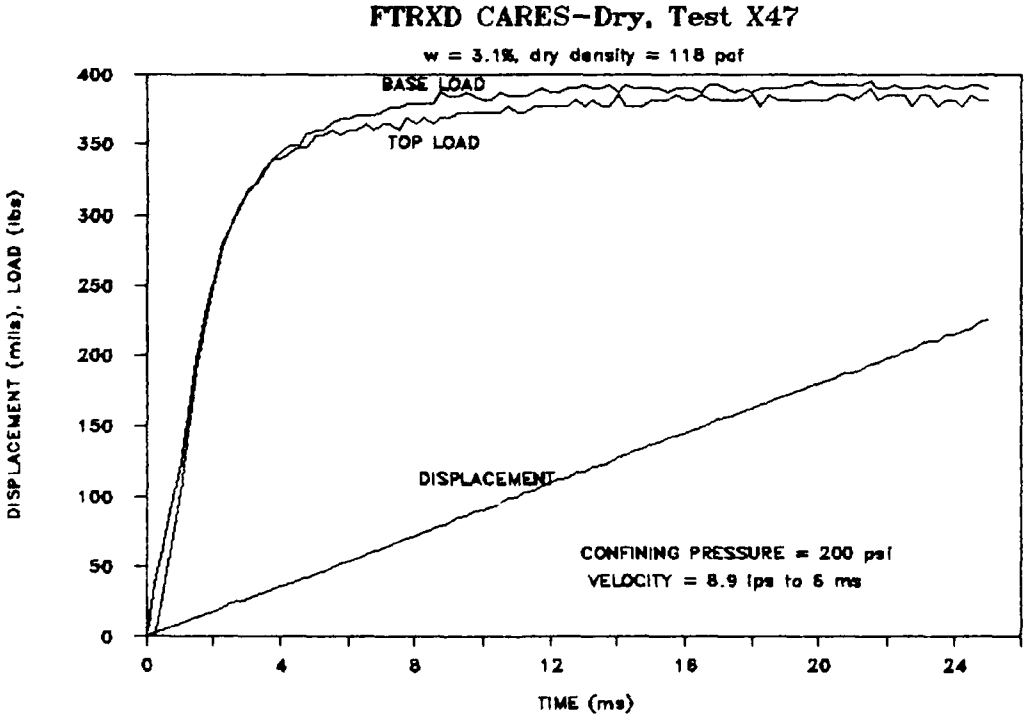

Figure 3.18, LOAD-DISPLACEMENT-TIME
(CP = 200 psi; VEL = 9.2 and 8.9 ips)

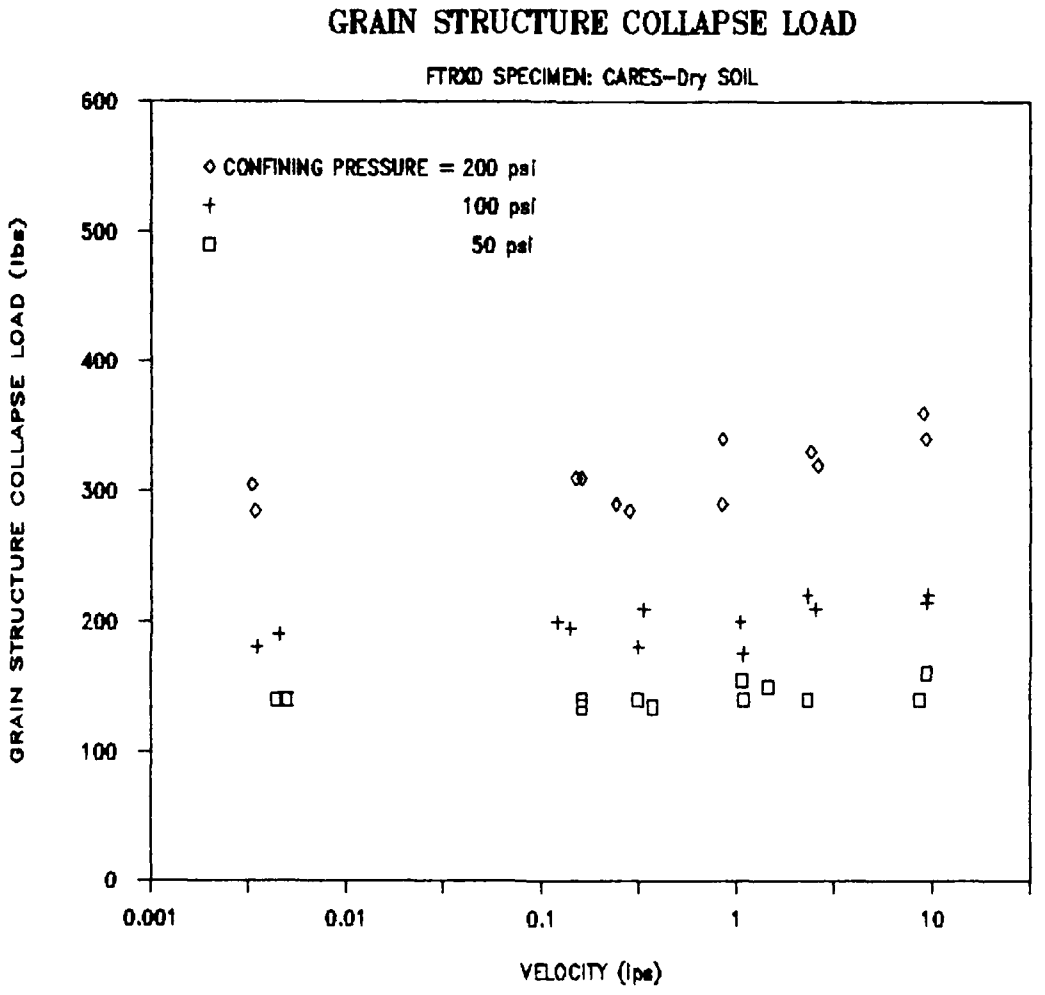

Figure 3.19, GRAIN STRUCTURE COLLAPSE LOAD

STRESS-STRAIN SUMMARY

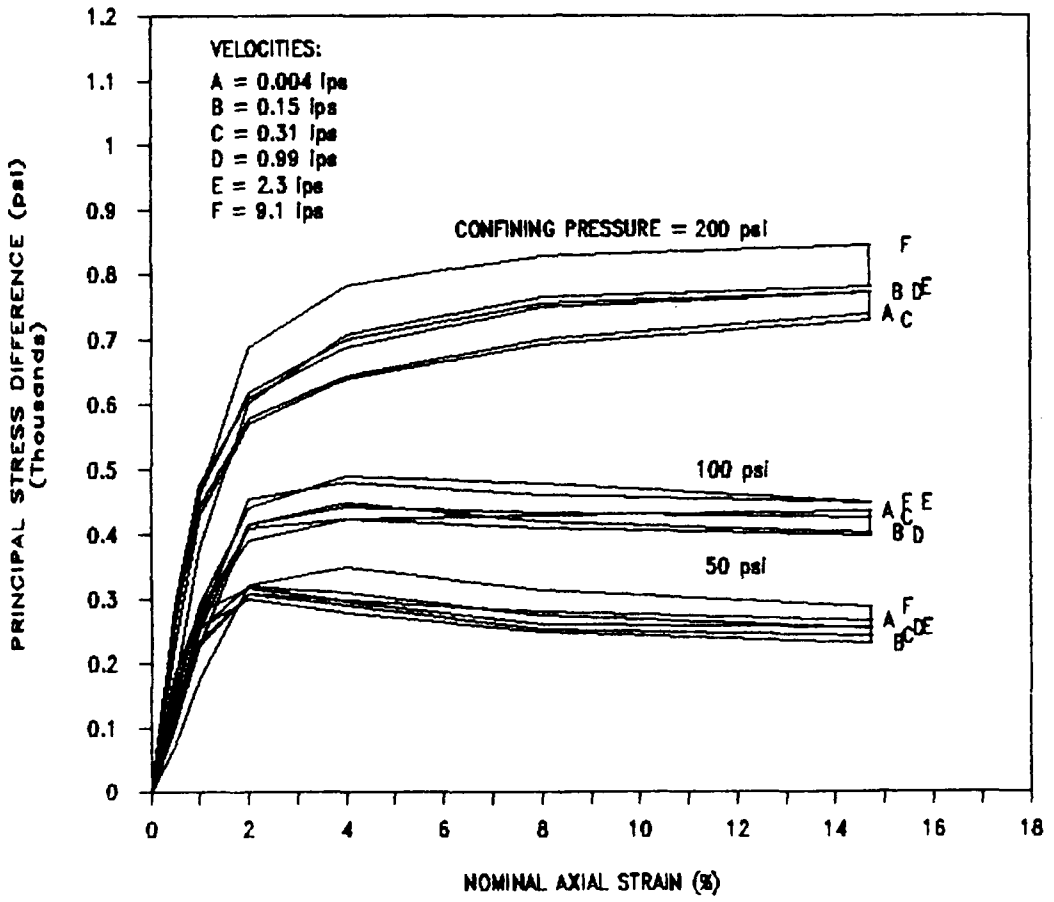

Figure 3.20, STRESS-STRAIN SUMMARY

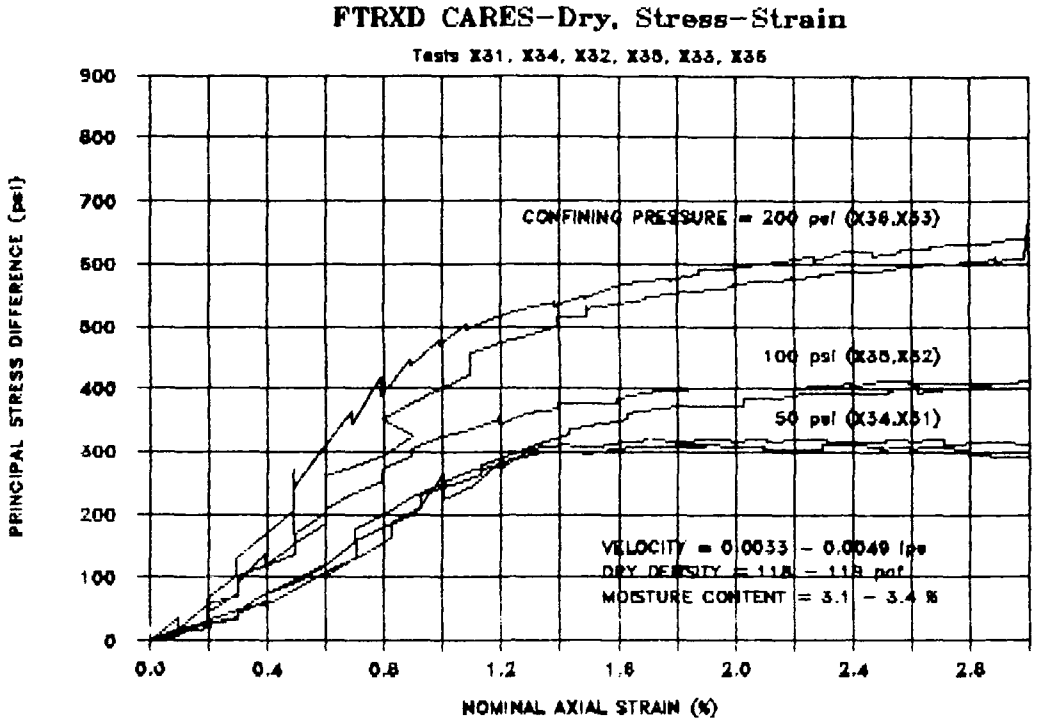

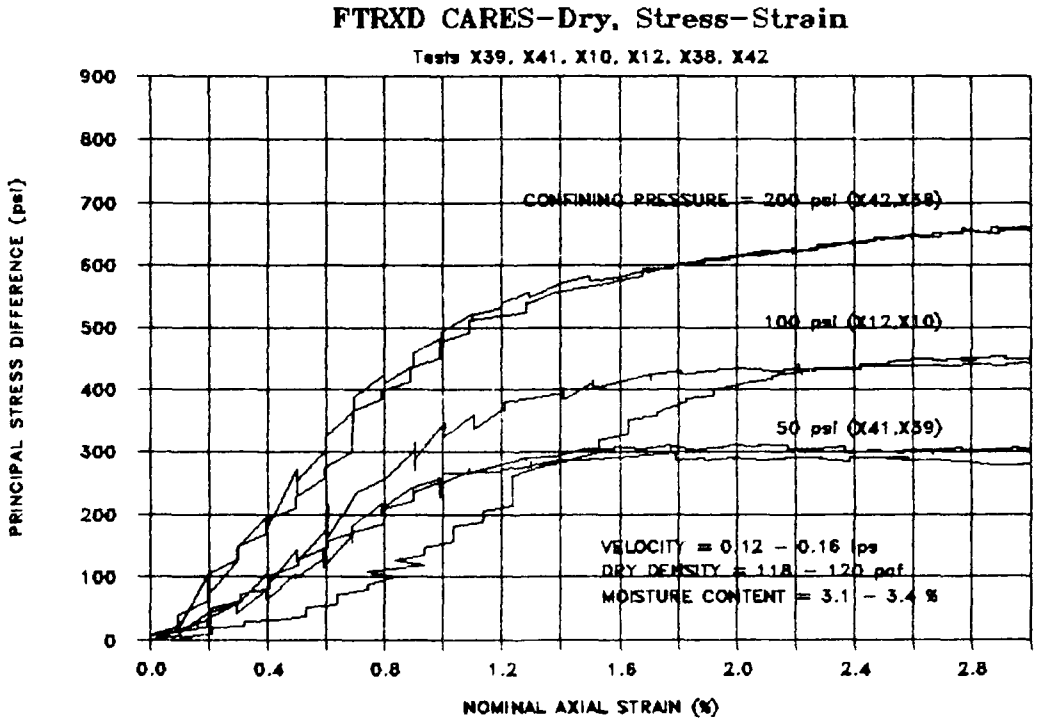

Fig 3.21, PRINCIPAL STRESS DIFFERENCE–NOMINAL AXIAL STRAIN
(VEL = 0.0033 – 0.0047 ips & VEL = 0.12 – 0.16 ips)

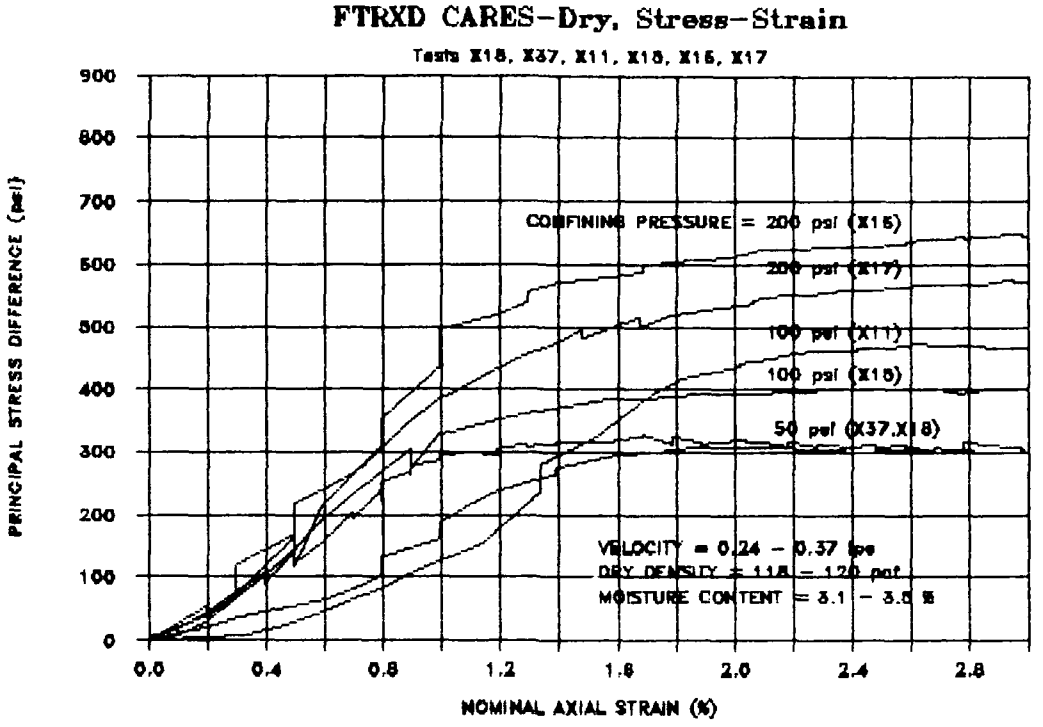

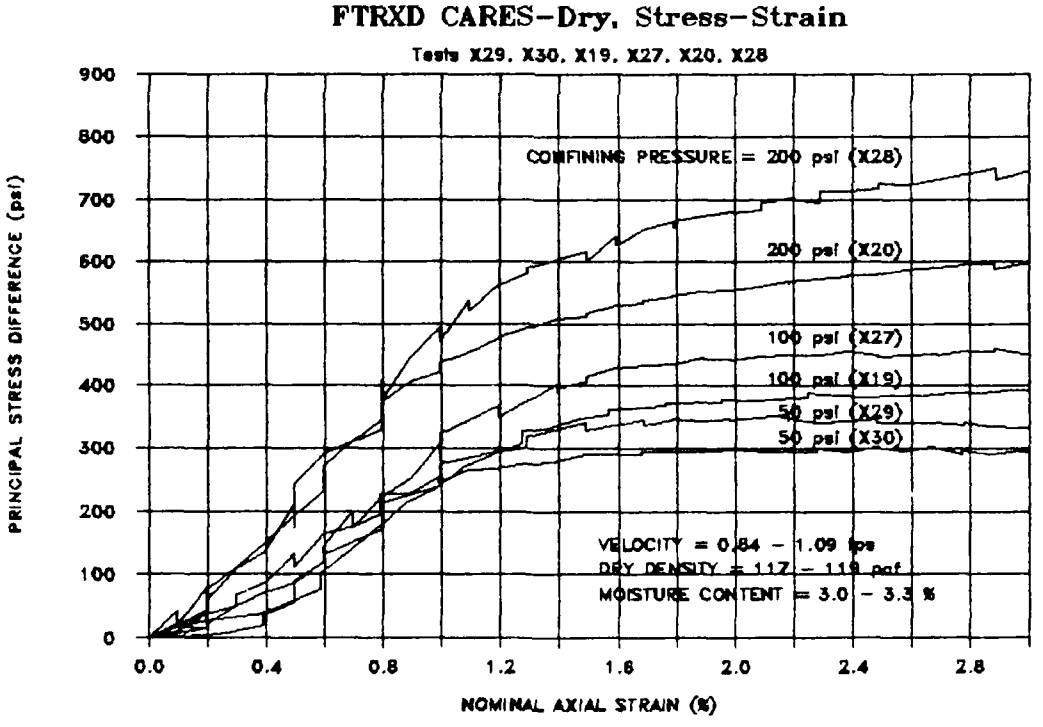

Fig 3.22, PRINCIPAL STRESS DIFFERENCE-NOMINAL AXIAL STRAIN (VEL = 0.24 – 0.37 ips and VEL = 0.84 – 1.09 ips)

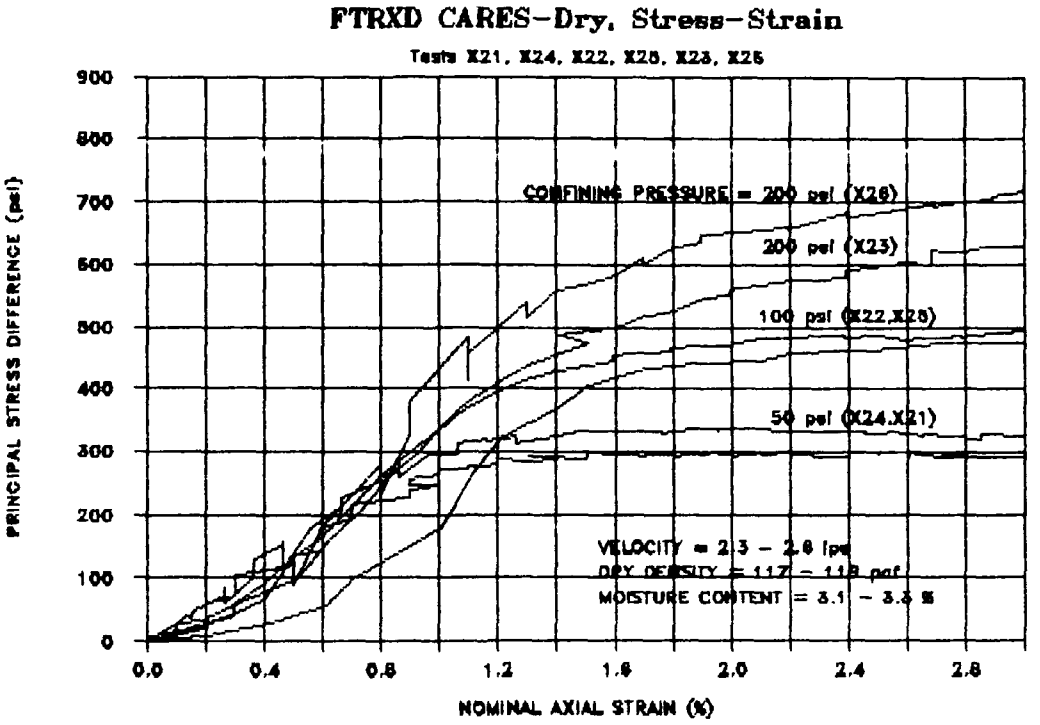

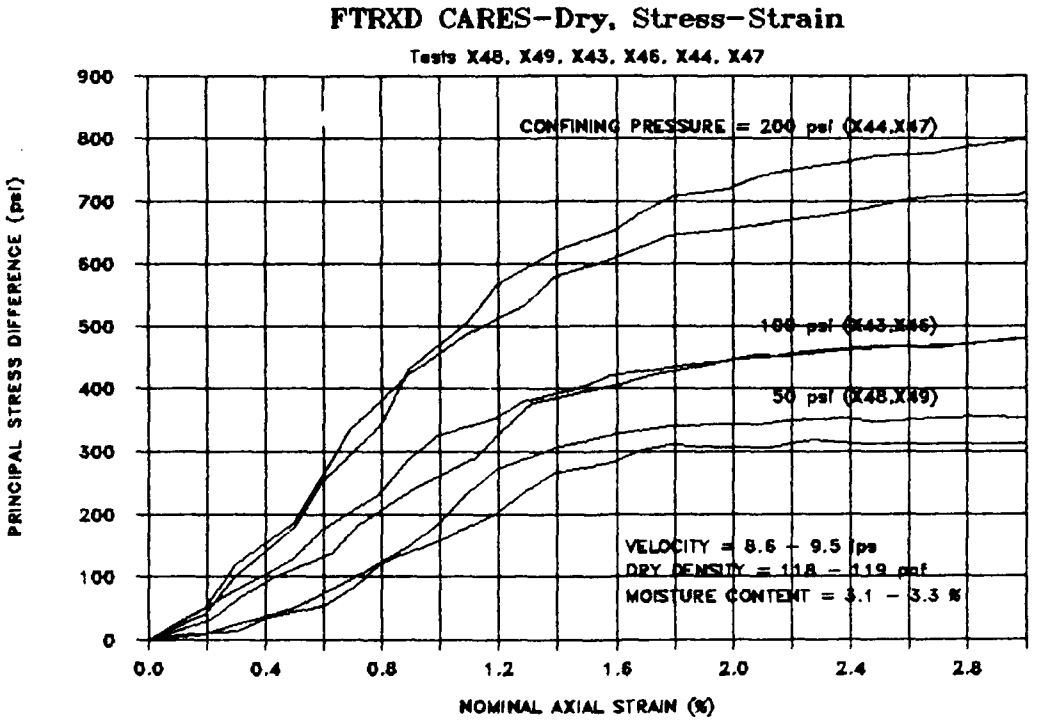

Fig 3.23, PRINCIPAL STRESS DIFFERENCE-NOMINAL AXIAL STRAIN (VEL = 2.3 - 2.6 ips and VEL = 8.6 - 9.5 ips)

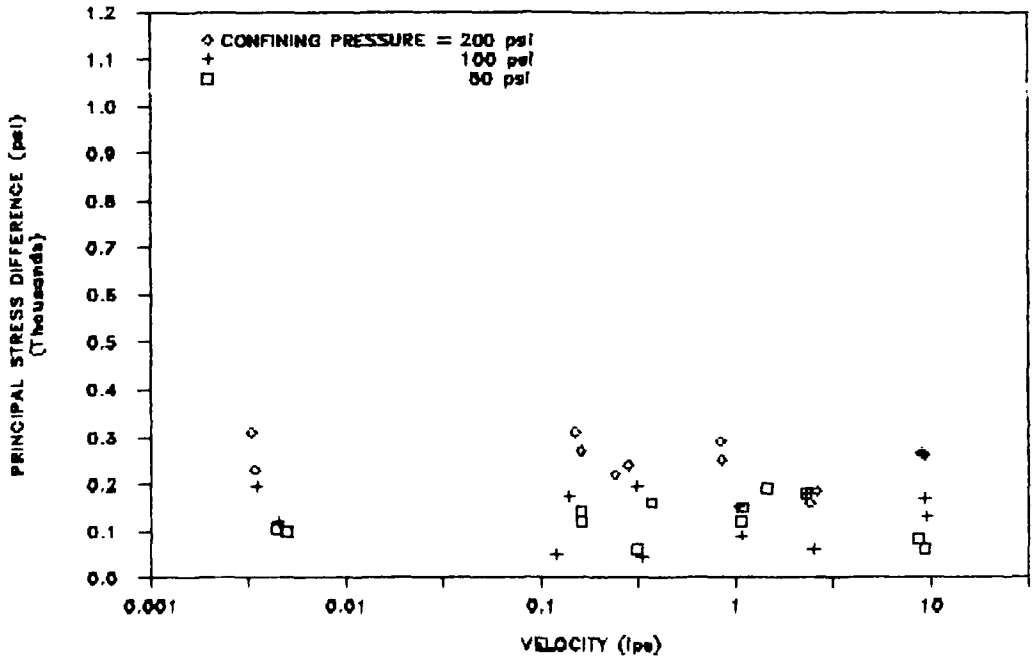

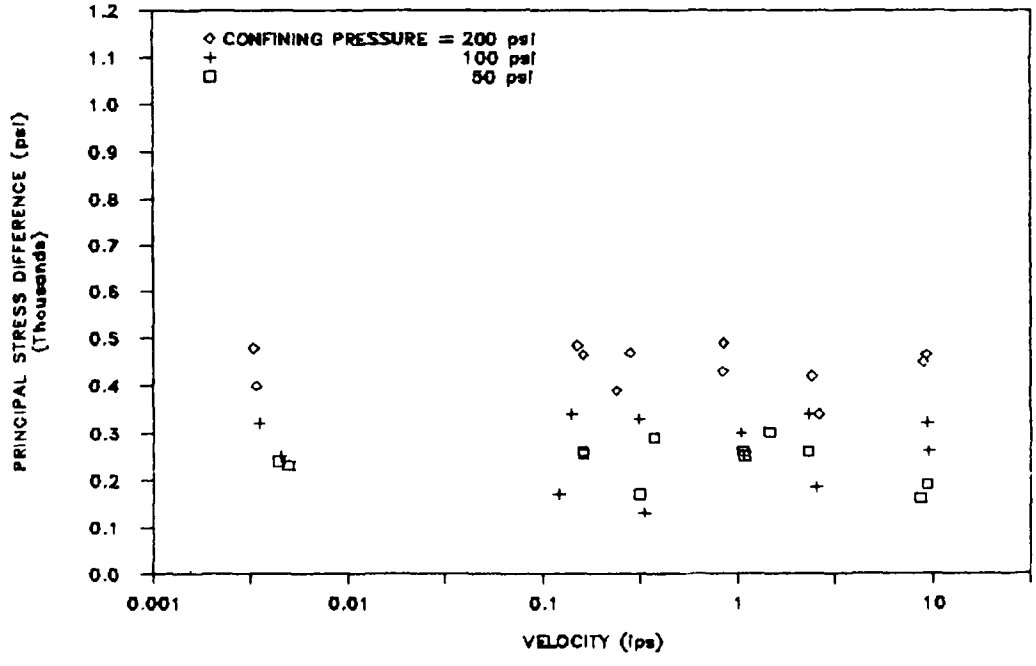

Figure 3.24, STRESS LEVEL-VELOCITY PLOTS
for NAS = 0.5% and 1.0%

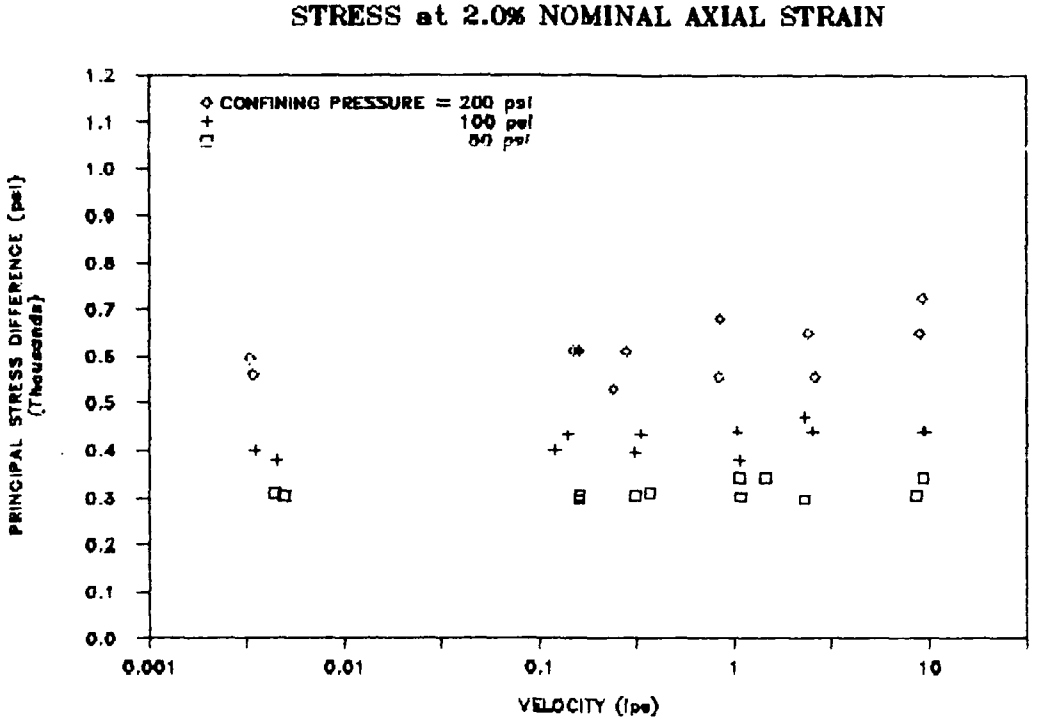

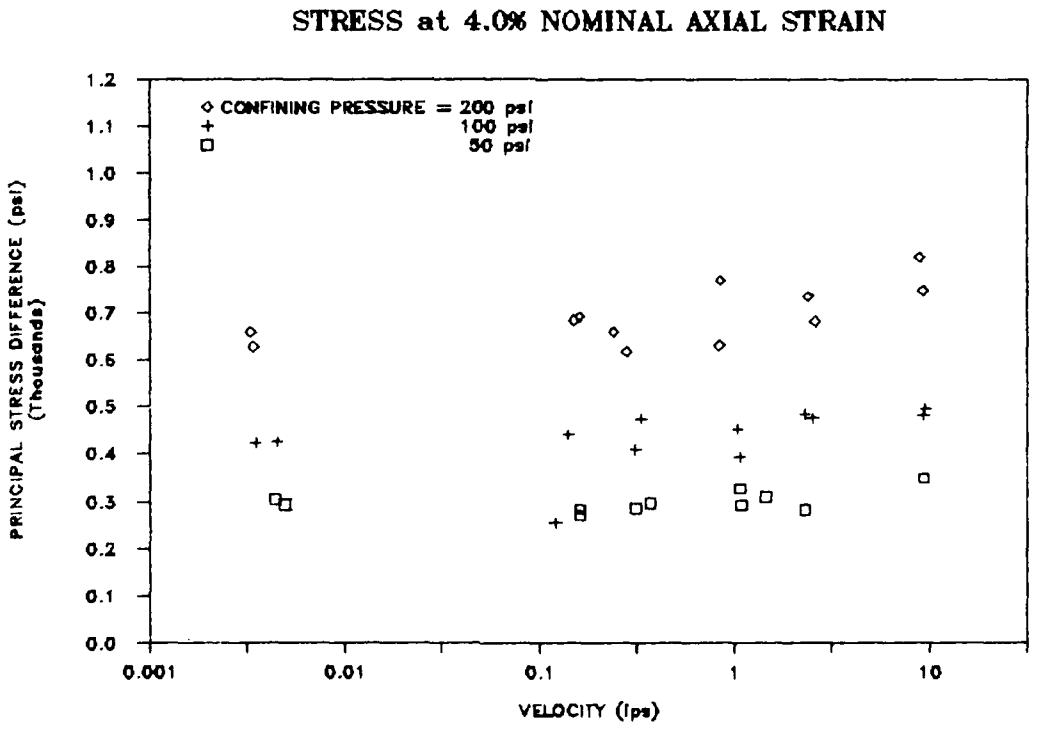

Figure 3.25, STRESS LEVEL-VELOCITY PLOTS
for NAS = 2.0% and 4.0%

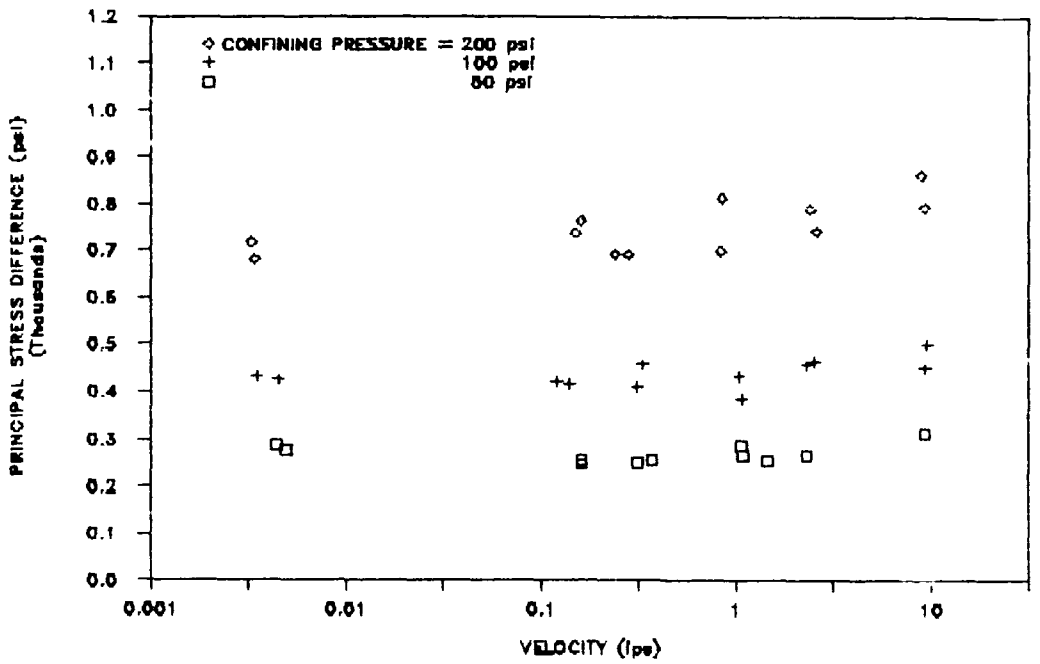

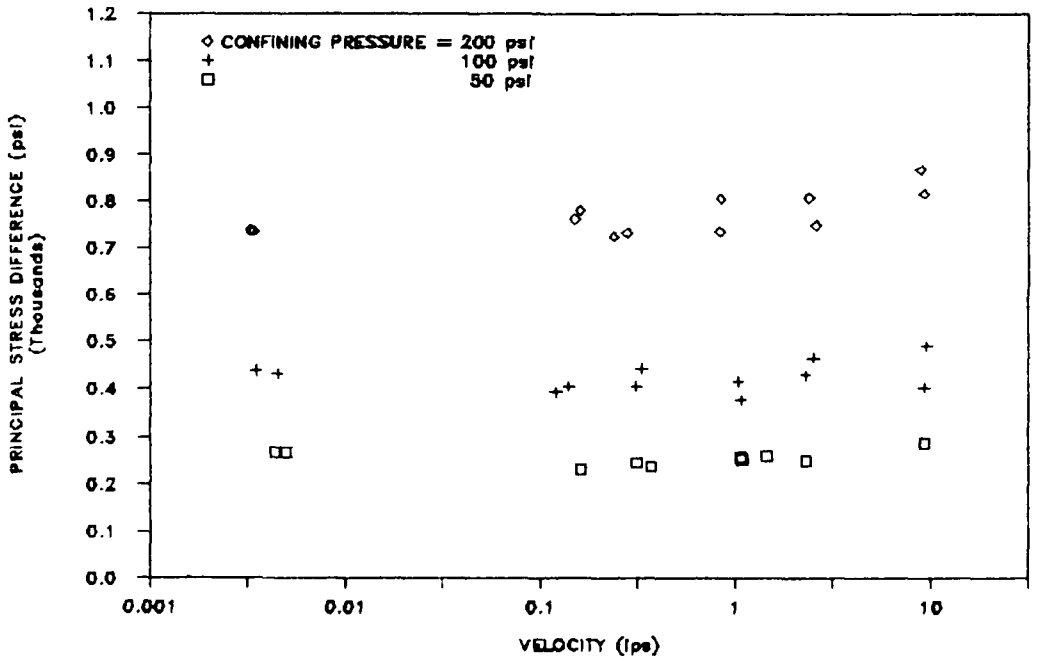

Figure 3.26, STRESS LEVEL-VELOCITY PLOTS
for NAS = 8.0% and 15.0%

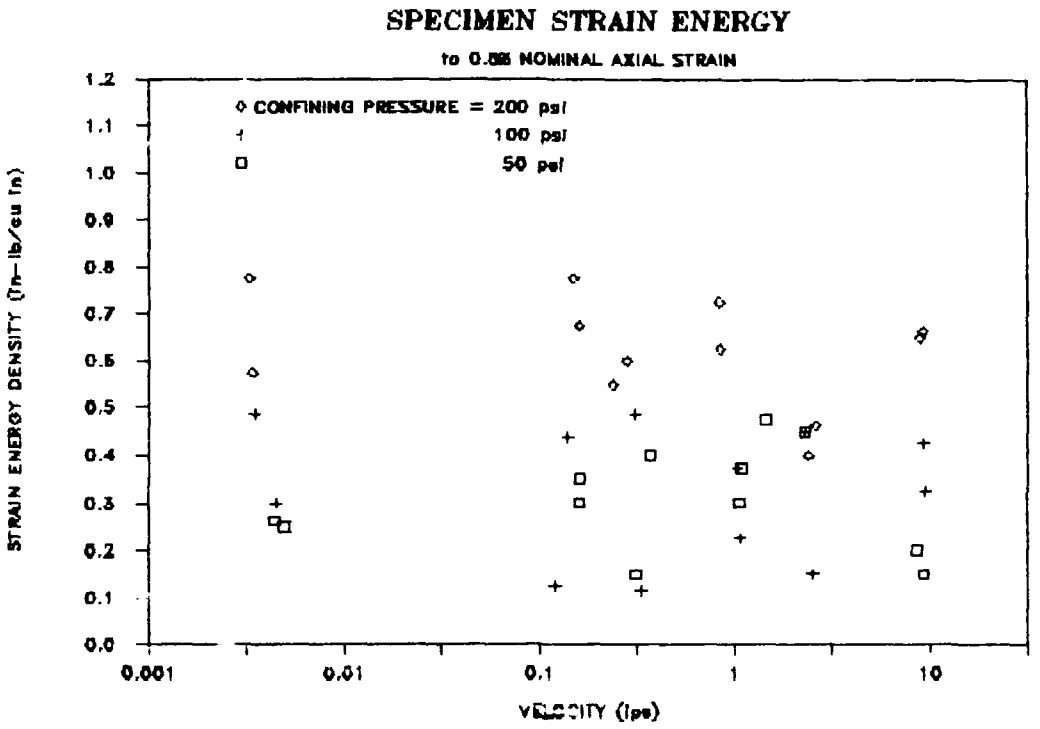

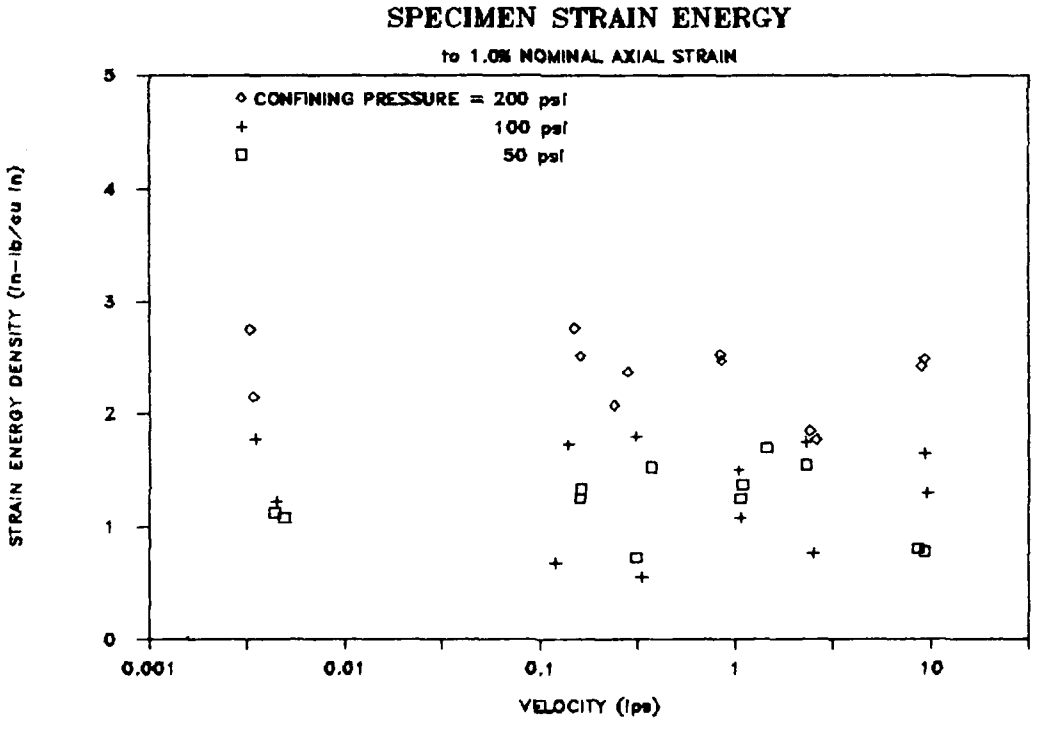

Figure 3.27, STRAIN ENERGY-VELOCITY PLOTS
for NAS = 0.5% and 1.0%

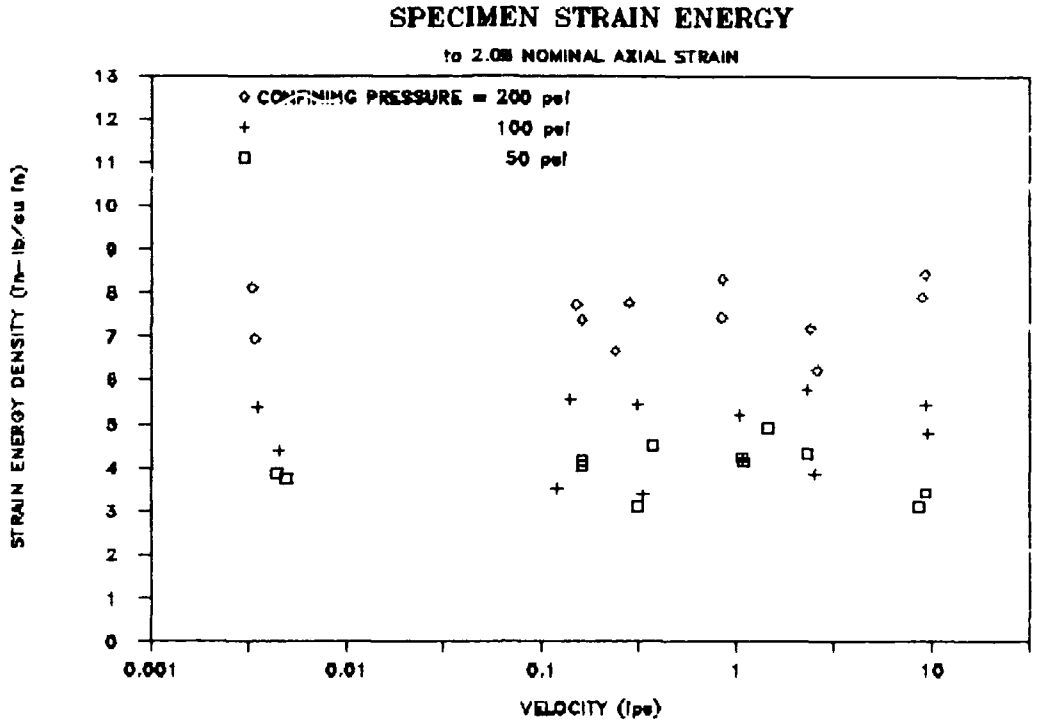

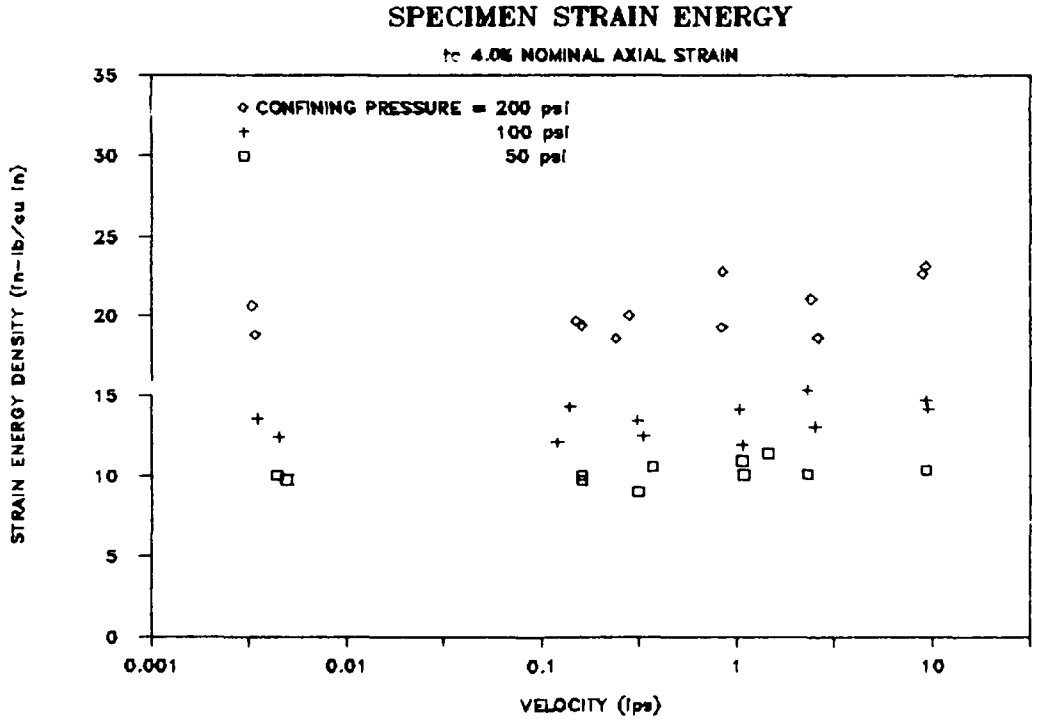

Figure 3.28, STRAIN ENERGY-VELOCITY PLOTS for NAS = 2.0% and 4.0%

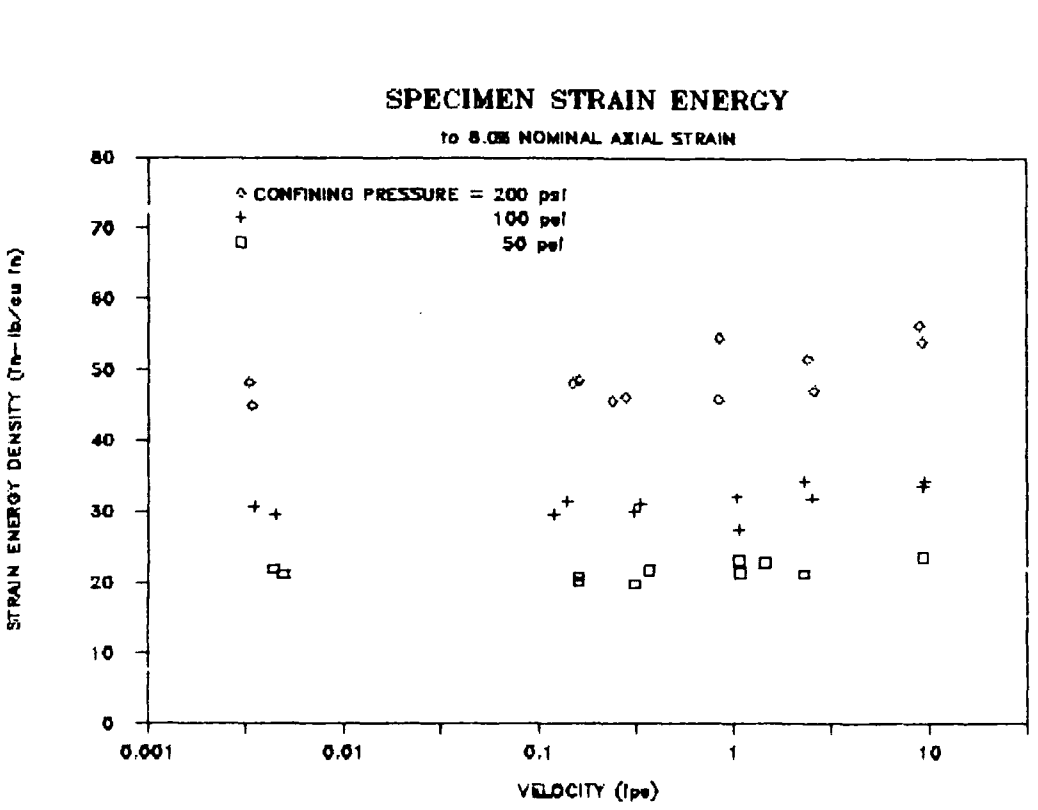

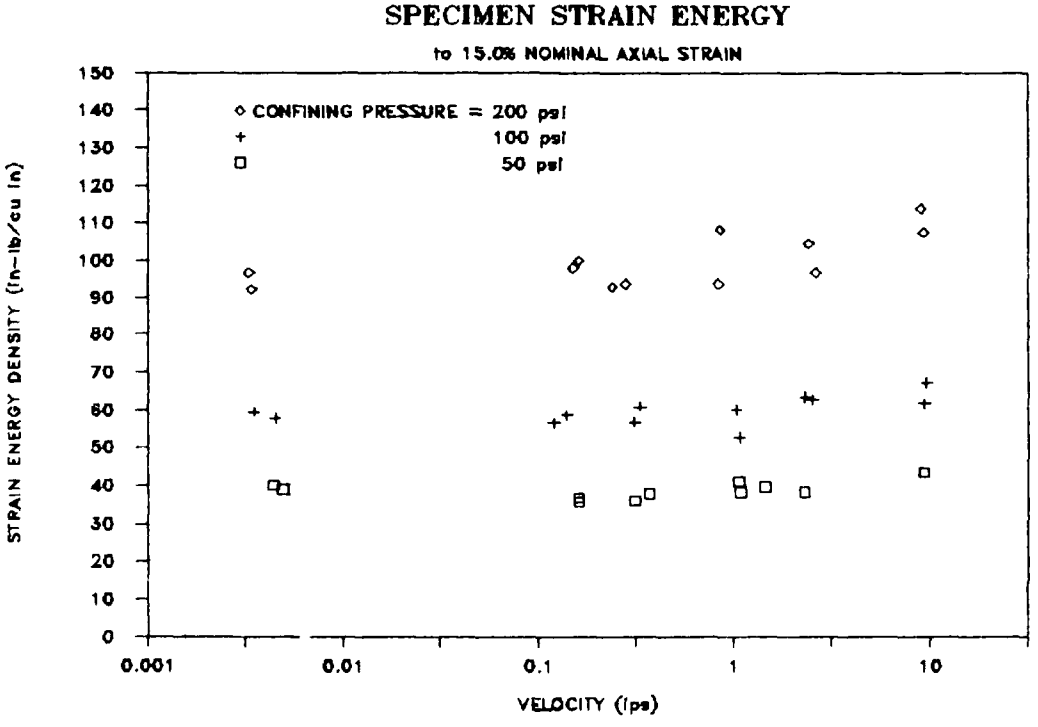

Figure 3.29, STRAIN ENERGY-VELOCITY PLOTS
for NAS = 8.0% and 15.0%

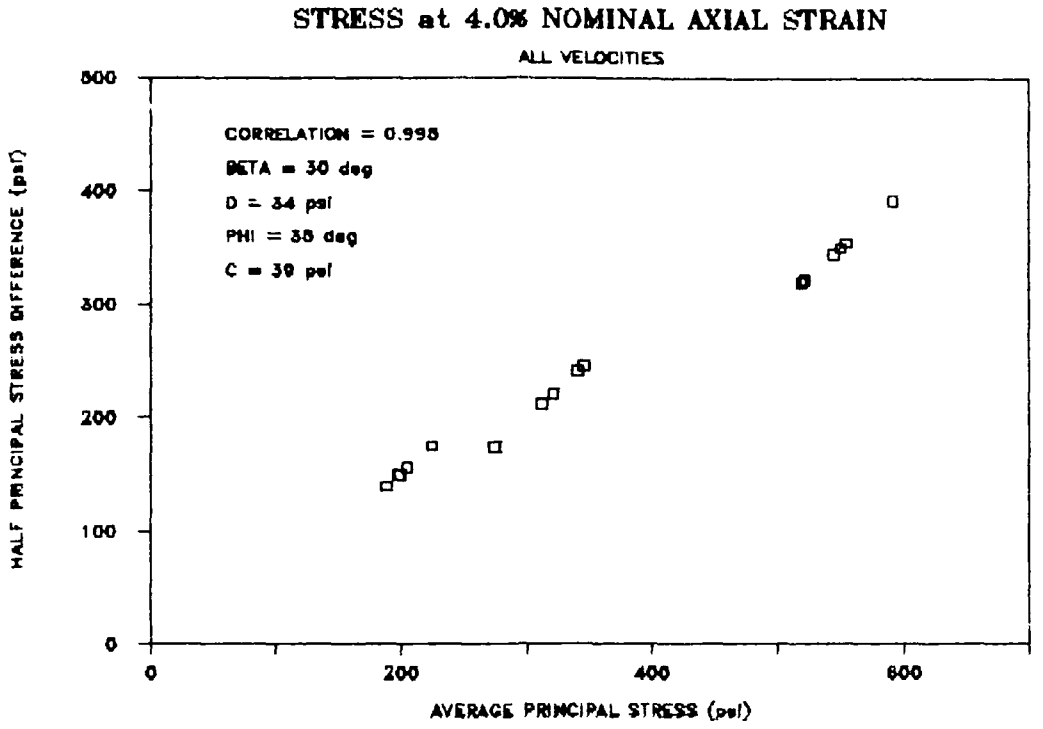

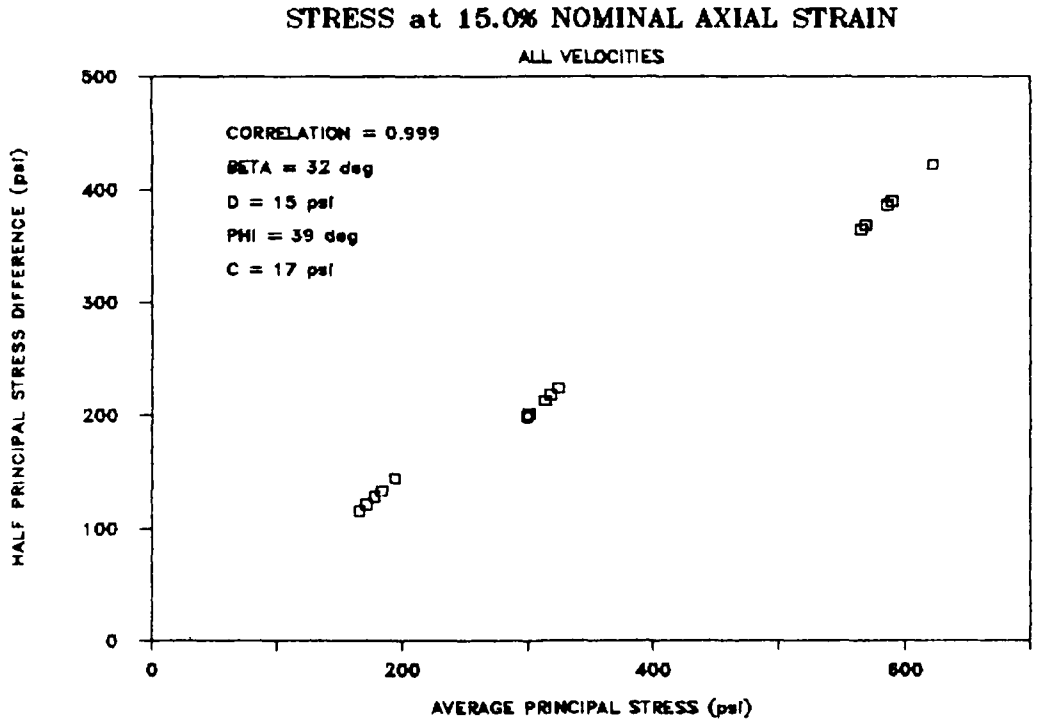

Figure 3.30, STRENGTH ENVELOPES

CHAPTER 4

SUMMARY, CONCLUSIONS, and RECOMMENDATIONS

Thirty-six individual specimens of CARES-Dry soil were tested in the FTRXD at confining pressures of 50, 100, and 200 psi and at nominal piston-ram velocities of 0.003, 0.15, 0.30, 1.0, 2.5, and 9.0 ips. The slowest tests took about 80 sec to achieve 15% NAS and were considered to be static, unconsolidated, undrained triaxial compression tests. The fastest tests (3000 times faster than the slowest) took about 25 msec to reach 15% NAS; this axial strain rate was the fastest that could be obtained with the FTRXD in its present configuration and still maintain constant deformation velocity throughout the test.

The FTRXD performed well. Load and displacement as a function of time were recorded with sufficient accuracy to determine the desired soil properties. The "identical" specimen pairs showed almost identical load and deformation responses. The differences that did occur were small and are attributed more to differences in the soil specimens themselves than to effects of the FTRXD. Constant velocities were achieved in each test and were reasonably close to the magnitudes desired. Procedures developed to prepare specimens, mount them in the FTRXD, and assemble and operate the FTRXD were reasonably efficient. The most difficult activity in these operating procedures was obtaining good specimen alignment with the load cells while ensuring that the piston-ram was in the proper position and that neither were disturbed during assembly. This difficulty could be greatly reduced by modifying the FTRXD so that the specimen and lower load cell could be moved up or down gently through a range of 500 mils after the FTRXD is assembled.

The new upper load cell was accurate, durable, and easy to use. During this test series, the earlier recorded consistent discrepancies between the upper and lower load cells were essentially eliminated, perhaps due to the new upper load cell. However, it was essential to exercise great care in determining when specimen deformation began in each test if there was to be agreement between the load cells.

Neither the dynamics of the FTRXD nor specimen inertia influenced the test results noticeably, despite the fact that some specimens were brought to failure in 2 to 3 msec. In the most rapid tests, a minor lag in the response of the lower load cell was detected which represented the time it took for the initial disturbance at the top of the specimen to propagate the length of the specimen. Consequently, faster test velocities or longer test specimens will require that specimen inertia be taken into account in ways such as those described in Reference 1.

The FTRXD does permit assessing rate effects of soils subjected to triaxial shear throughout meaningful ranges of principal stress difference (PSD) and nominal axial strain (NAS). During deformation, the CARES-Dry soil appeared to pass through three behavior modes, i.e., (1) initial grain structure response from 0-1% NAS, (2) grain structure collapse from 1-4% NAS, and (3) plastic shear failure from 4-15% NAS.

During the first mode, the grain structure of the specimen is intact, and the relationship between PSD and NAS is essentially linear, increases predictably with increasing confining pressure, and at high confining pressure is not affected by deformation velocity. At low confining pressure when deformation velocity is high, the results were varied and inconclusive.

The second mode when the grain structure is collapsing and the third mode when plastic shear behavior dominates show the same effects of deformation velocity. The PSD-NAS relationship is highly nonlinear during the second mode but approaches linearity during the third. Increasing confining pressure increases the magnitudes of PSD in a predictable manner in both modes, and there is a modest increase in PSD at high confining pressure due to deformation velocity. Rate effects were not observed in these modes at the lower confining pressures.

The CARES-Dry soil at the test series moisture content and dry density has single linear Coulomb failure envelopes for particular values of NAS from 4-15%, although the envelopes are not quite the same at different values of NAS. The observed increase in PSD in this range of NAS due to deformation velocity is not reflected on the envelope. The increase causes both the shear strength and the average principal stress to increase equally, so that within the accuracy of the test data these increases track close to the envelope.

The test series moisture content (3.2%) and dry density (118.5 pcf) were slightly different from those used in uniaxial strain compression testing for rate effects in the CARES-Dry soil (3.5%, 115 pcf) as described in Reference 3. However, the rate effects observed during testing with FTRXD were small enough to suggest that small changes in moisture content and dry density ought not to influence rate effects significantly so that the FTRXD results might be compared with the uniaxial strain compression results. However, further testing in the FTRXD will be necessary to achieve deformation velocities comparable to the fastest velocities achieved in the uniaxial strain compression device; deformation velocities of 35 to 50 ips in the FTRXD will be required.

Based on the results obtained and the experience gained during this test series, the following recommendations are made in order to improve and extend the results obtained from future test series:

(1). Install a mechanism at the base of the lower load cell in the FTRXD that will allow the lower load cell with the specimen mounted on it to be raised and lowered through a range of 0.5 inches (500 mils). The mechanism should be manually controlled from outside the triaxial chamber; it should not rotate, jostle, or otherwise disturb the specimen as it moves up or down. It must be rigid enough to hold the specimen steady and sturdy enough to withstand the loads imposed during testing. The purpose of the mechanism is to allow the gentle and precise seating of the piston-ram on the upper load cell after the FTRXD is assembled, or the precise setting of the back-off distance of the piston-ram from the specimen. This will permit improved determination of the start of deformation of the specimen and therefore improved test data at very low nominal axial strains. Moreover, it will also allow the test operator to minimize the possibility of specimen disturbance or misalignment during the assembly process.

(2). Install an accelerometer on the piston-ram. For testing when specimen inertia is not significant, such as in the current test series, an accelerometer on the piston-ram would greatly assist in determining when specimen deformation begins. For more rapid testing, such as is anticipated in the future, an accelerometer on the piston-ram will also greatly assist in defining the motion of the top of the specimen. The nature of this motion plays a dominant role in deducing the constitutive behavior of the specimen from the load cell and displacement gage readings.

(3). Install a two tube manifold on the lower chamber of the load cylinder with larger tubing and orifices than the current single line uses. The manifold should feed into a single large diameter exhaust tube and be controlled by a single solenoid valve with an opening larger than the current one. The exit orifices and manifold tubing from the lower chamber of the load cell should be at least twice the inside diameter of the current single orifice and line. The two orifices should be diametrically opposite to one another. The number of turns in the tubing and their severity should be minimized. The inside diameter of the single exhaust tube should be twice the inside diameter of the tubing used for the manifold. The opening in the solenoid valve must be at least as large as the inside diameter of the single exhaust tube. This represents an eight-fold increase in the area through which oil flows from the lower chamber of the load cylinder during testing, and

given the likely head losses during flow should result in maximum constant test velocities of about 35 to 50 ips.

(4) Extend the current test series on CARES-Dry soil to test specimens at faster deformation rates -- up to 50 ips.

* First with the FTRXD modified as recommended in (1)-(3) above using oil in the lower chamber of the load cylinder so that constant deformation velocities are possible.

* Second with the FTRXD modified as recommended in (1)-(2) above but with no oil in the lower chamber of the load cylinder and this chamber open to the atmosphere. In this second series, an effort would be made to determine an "effective" deformation velocity from the variable test velocity that occurs.

REFERENCES

[1] Carroll, William F., January 1988, "Fast Triaxial Shear Device Evaluation," Technical Report SL-88-2 , US Army Engineer Waterways Experiment Station, Vicksburg, MS.

[2] Cargile, James D., September 1986, "Geotechnical Investigation for the CARES-Dry Site; Report 2, Laboratory Test Results", Technical Report SL86-16, US Army Engineer Waterways Experiment Station, Vicksburg, MS.

[3] Farr, John V., December 1986, "Loading Rate Effects on the One-Dimensional Compressibility of Four Partially Saturated Soils," Technical Report SL-86-46, US Army Engineer Waterways Experiment Station, Vicksburg, MS.

DISTRIBUTION LIST

DEPARTMENT OF DEFENSE

Director
Defense Nuclear Agency
ATTN: DFSP (Dr. C. W. Ullrich)
SPSD (MAJ M. A. Reed)
SPWE (Dr. C. Canada)
SPWE (MAJ M. Pelkey)
Technical Library
Washington, DC 20305-1000

Defense Nuclear Agency
Nevada Operations Office
ATTN: TDNV (Mr. J. W. LaComb)
P. O. Box 208
Mercury, NV 89023

Director
Defense Advanced Research Project Agency
ATTN: Technical Library
1400 Wilson Blvd.
Arlington, VA 22209

Director
Defense Intelligence Agency
ATTN: Technical Library
Washington, DC 20301-6111

Defense Technical Information Center
Cameron Station
ATTN: TC (2 cys)
Alexandria, VA 22314

DEPARTMENT OF THE ARMY

Commander
US Army Corps of Engineers
ATTN: CERD-L (Ms. Sharon Vannucci)
CERD-M (Mr. B. O. Benn)
CEEC-ET (Mr. R. L. Wight)
CEIM-SL
Washington, DC 20314-1000

Division Engineer
US Army Engineer Division, Huntsville
ATTN: CEHND-SR
P. O. Box 1600, West Station
Huntsville, AL 35807-4301

District Engineer
US Army Engineer District, Omaha
ATTN: CEMRO-ED-S (Mr. Bob Kelley)
CEMRO-ED-SH (Mr. Bill Gaube)
215 N. 17th Street
Omaha, NE 68102-4978

Director
US Army Construction Engineering
Research Laboratory
ATTN: Technical Library
P. O. Box 4005
Champaign, IL 61820-1305

Commander/Director
US Army Cold Regions Research and
Engineering Laboratory
ATTN: Technical Library
72 Lyme Road
Hanover, NH 03755-1290

Commandant
US Army Engineer School
ATTN: ATZA-CD (COL Fred Parker)
Technical Library
Ft. Belvoir, VA 22060-5281

Commander
US Army Laboratory Command
ATTN: Technical Library
2800 Powder Mill Road
Adelphi, MD 20783-1145

Director
US Army Ballistic Research Laboratory
ATTN: Technical Library
Aberdeen Proving Ground, MD 21005-5066

Commander
US Army Nuclear and Chemical Agency
ATTN: Technical Library
7500 Backlick Road, Bldg. 2073
Springfield, VA 22150

DEPARTMENT OF THE NAVY

Naval Civil Engineering Laboratory
ATTN: Technical Library
Port Hueneme, CA 93043

Naval Facilities Engineering Command
ATTN: Technical Library
200 Stovall Street
Alexandria, VA 22332

DEPARTMENT OF THE AIR FORCE

Air Force Institute of Technology
Air University
ATTN: Technical Library
Wright-Patterson Air Force Base, OH 45433

Air Force Office of Scientific Research
ATTN: Technical Library
Bolling Air Force Base, DC 20332

Air Force Weapons Laboratory (AFSC)
ATTN: NTESG (CPT C. W. Felice)
Technical Library
Kirtland Air Force Base, NM 87117-6008

Air Force Engineering and Services
Center (AFSC)
ATTN: Technical Library
Tyndall Air Force Base, FL 32403

Air Force Armament Laboratory (AFSC)
ATTN: Technical Library
Eglin Air Force Base, FL 32542

DEPARTMENT OF THE AIR FORCE (Continued)

Commander
Ballistic Missile Office (AFSC)
ATTN: MYEB (LTC D. H. Gage)
Technical Library
Norton Air Force Base, CA 92409

DEPARTMENT OF ENERGY

Lawrence Livermore National Laboratory
ATTN: Technical Library
P. O. Box 808
Livermore, CA 94550

Los Alamos National Laboratory
ATTN: Technical Library
P. O. Box 1663
Los Alamos, NM 87545

Sandia National Laboratories
ATTN: Technical Library
P. O. Box 5800
Albuquerque, NM 87185

Sandia National Laboratories
ATTN: Technical Library
Livermore, CA 94550

DEPARTMENT OF DEFENSE CONTRACTORS

Mr. J. L. Bratton
Applied Research Associates, Inc.
4300 San Mateo Blvd., NE, Suite A220
Albuquerque, NM 87110

Mr. J. D. Shinn
Applied Research Associates, Inc.
South Royalton, VT 05068

Mr. J. L. Drake
Applied Research Associates, Inc.
3202 Wisconsin Avenue
Vicksburg, MS 39180-2610

Dr. J. G. Trulio
Applied Theory, Inc.
930 S. LaBrea Avenue
Los Angeles, CA 90036

Dr. Y. Marvin Ito
California Research & Technology, Inc.
20943 Devonshire Street
Chatsworth, CA 91311-2376

Dr. E. J. Rinehart
California Research & Technology, Inc.
2017 Yale Blvd., SE
Albuquerque, NM 87106

Dr. Hon-Yim Ko
Department of Civil, Environmental, and
Architectural Engineering
University of Colorado at Boulder
Boulder, CO 80309

Dr. K. C. Valanis
Endochronics, Inc.
8605 Northwest Lakecrest Court
Vancouver, WA 98665

Technical Library
New Mexico Engineering Research Institute
University of New Mexico
Box 25, University Station
Albuquerque, NM 87131

Dr. Don Simons
R&D Associates
P. O. Box 9695
Marina del Rey, CA 90291

Mr. L. S. Melzer
Science Applications International
Corporation
505 West Texas Street
First City Center, Tower 2, Suite 1335
Midland, TX 79701

Dr. John Schatz
Science Applications International
Corporation
P. O. Box 2351
La Jolla, CA 92038-2351

Dr. H. E. Read
S-Cubed
P. O. Box 1620
La Jolla, CA 92038-1620

Dr. Lynn Seaman
SRI International
333 Ravenswood Avenue
Menlo Park, CA 94025

Mr. S. J. Green
Terra Tek, Inc.
420 Wakara Way
Salt Lake City, UT 84108

Dr. M. G. Katona
TRW Defense Systems Group
P. O. Box 1310
San Bernardino, CA 92402

Dr. I. S. Sandler
Weidlinger Associates
333 Seventh Avenue
New York, NY 10001

Dr. W. F. Carroll (10 cys)
Department of Civil Engineering
and Environmental Sciences
University of Central Florida
Orlando, FL 32816

END

DATE

FILMED

DTIC

JULY 88